EUROPEAN ORGANIZATION FOR NUCLEAR RESEARCH

CERN–PPE/96-06

25 January 1996

Measurement of the B_d^0 oscillation frequency using kaons, leptons and jet charge

DELPHI Collaboration

Abstract

A measurement of the mass difference, Δm_d, between the two physical B_d^0 states has been obtained from the analysis of the impact parameter distribution of a lepton emitted at large transverse momentum (p_t) relative to the jet axis and from the analysis of the flight distance distribution of secondary vertices tagged by either a high p_t lepton or an identified kaon. In the opposite hemisphere of the event, the charge of the initial quark has been evaluated using a high p_t lepton, a charged kaon or the mean jet charge. With 1.7 million hadronic Z^0 decays recorded by DELPHI between 1991 and 1993, Δm_d is found to be:

$$\Delta m_d = 0.531^{+0.050}_{-0.046}\ (stat.) \pm 0.078\ (syst.)\ \mathrm{ps}^{-1}\ .$$

(To be submitted to Zeit f. Physik C.)

P.Abreu[21], W.Adam[50], T.Adye[37], E.Agasi[31], I.Ajinenko[42], R.Aleksan[39], G.D.Alekseev[16], R.Alemany[49], P.P.Allport[22], S.Almehed[24], U.Amaldi[9], S.Amato[47], A.Andreazza[28], M.L.Andrieux[14], P.Antilogus[9], W-D.Apel[17], Y.Arnoud[39], B.Åsman[44], J-E.Augustin[19], A.Augustinus[9], P.Baillon[9], P.Bambade[19], R.Barate[14], M.Barbi[47], D.Y.Bardin[16], A.Baroncelli[40], O.Barring[24], J.A.Barrio[26], W.Bartl[50], M.J.Bates[37], M.Battaglia[15], M.Baubillier[23], J.Baudot[39], K-H.Becks[52], M.Begalli[6], P.Beilliere[8], Yu.Belokopytov[9,53], A.C.Benvenuti[5], M.Berggren[47], D.Bertrand[2], F.Bianchi[45], M.Bigi[45], M.S.Bilenky[16], P.Billoir[23], D.Bloch[10], M.Blume[52], S.Blyth[35], T.Bolognese[39], M.Bonesini[28], W.Bonivento[28], P.S.L.Booth[22], G.Borisov[42], C.Bosio[40], S.Bosworth[35], O.Botner[48], E.Boudinov[31], B.Bouquet[19], C.Bourdarios[9], T.J.V.Bowcock[22], M.Bozzo[13], P.Branchini[40], K.D.Brand[36], T.Brenke[52], R.A.Brenner[15], C.Bricman[2], L.Brillault[23], R.C.A.Brown[9], P.Bruckman[18], J-M.Brunet[8], L.Bugge[33], T.Buran[33], T.Burgsmueller[52], P.Buschmann[52], A.Buys[9], S.Cabrera[49], M.Caccia[28], M.Calvi[28], A.J.Camacho Rozas[41], T.Camporesi[9], V.Canale[38], M.Canepa[13], K.Cankocak[44], F.Cao[2], F.Carena[9], L.Carroll[22], C.Caso[13], M.V.Castillo Gimenez[49], A.Cattai[9], F.R.Cavallo[5], L.Cerrito[38], V.Chabaud[9], Ph.Charpentier[9], L.Chaussard[25], J.Chauveau[23], P.Checchia[36], G.A.Chelkov[16], M.Chen[2], R.Chierici[45], P.Chliapnikov[42], P.Chochula[7], V.Chorowicz[9], J.Chudoba[30], V.Cindro[43], P.Collins[9], J.L.Contreras[19], R.Contri[13], E.Cortina[49], G.Cosme[19], F.Cossutti[46], H.B.Crawley[1], D.Crennell[37], G.Crosetti[13], J.Cuevas Maestro[34], S.Czellar[15], E.Dahl-Jensen[29], J.Dahm[52], B.Dalmagne[19], M.Dam[29], G.Damgaard[29], P.D.Dauncey[37], M.Davenport[9], W.Da Silva[23], C.Defoix[8], A.Deghorain[2], G.Della Ricca[46], P.Delpierre[27], N.Demaria[35], A.De Angelis[9], W.De Boer[17], S.De Brabandere[2], C.De Clercq[2], C.De La Vaissiere[23], B.De Lotto[46], A.De Min[36], L.De Paula[47], C.De Saint-Jean[39], H.Dijkstra[9], L.Di Ciaccio[38], F.Djama[10], J.Dolbeau[8], M.Donszelmann[9], K.Doroba[51], M.Dracos[10], J.Drees[52], K.-A.Drees[52], M.Dris[32], Y.Dufour[9], D.Edsall[1], R.Ehret[17], G.Eigen[4], T.Ekelof[48], G.Ekspong[44], M.Elsing[52], J-P.Engel[10], N.Ershaidat[23], B.Erzen[43], M.Espirito Santo[21], E.Falk[24], D.Fassouliotis[32], M.Feindt[9], A.Fenyuk[42], A.Ferrer[49], T.A.Filippas[32], A.Firestone[1], P.-A.Fischer[10], H.Foeth[9], E.Fokitis[32], F.Fontanelli[13], F.Formenti[9], B.Franek[37], P.Frenkiel[8], D.C.Fries[17], A.G.Frodesen[4], F.Fulda-Quenzer[19], J.Fuster[49], A.Galloni[22], D.Gamba[45], M.Gandelman[6], C.Garcia[49], J.Garcia[41], C.Gaspar[9], U.Gasparini[36], Ph.Gavillet[9], E.N.Gazis[32], D.Gele[10], J-P.Gerber[10], M.Gibbs[22], R.Gokieli[51], B.Golob[43], G.Gopal[37], L.Gorn[1], M.Gorski[51], Yu.Gouz[45,53], V.Gracco[13], E.Graziani[40], G.Grosdidier[19], K.Grzelak[51], S.Gumenyuk[28,53], P.Gunnarsson[44], M.Gunther[48], J.Guy[37], F.Hahn[9], S.Hahn[52], A.Hallgren[48], K.Hamacher[52], W.Hao[31], F.J.Harris[35], V.Hedberg[24], R.Henriques[21], J.J.Hernandez[49], P.Herquet[2], H.Herr[9], T.L.Hessing[35], E.Higon[49], H.J.Hilke[9], T.S.Hill[1], S-O.Holmgren[44], P.J.Holt[35], D.Holthuizen[31], S.Hoorelbeke[2], M.Houlden[22], J.Hrubec[50], K.Huet[2], K.Hultqvist[44], J.N.Jackson[22], R.Jacobsson[44], P.Jalocha[18], R.Janik[7], Ch.Jarlskog[24], G.Jarlskog[24], P.Jarry[39], B.Jean-Marie[19], E.K.Johansson[44], L.Jonsson[24], P.Jonsson[24], C.Joram[9], P.Juillot[10], M.Kaiser[17], F.Kapusta[23], K.Karafasoulis[11], M.Karlsson[44], E.Karvelas[11], S.Katsanevas[3], E.C.Katsoufis[32], R.Keranen[4], Yu.Khokhlov[42], B.A.Khomenko[16], N.N.Khovanski[16], B.King[22], N.J.Kjaer[29], H.Klein[9], A.Klovning[4], P.Kluit[31], B.Koene[31], P.Kokkinias[11], M.Koratzinos[9], K.Korcyl[18], C.Kourkoumelis[3], O.Kouznetsov[13,16], P.-H.Kramer[52], M.Krammer[50], C.Kreuter[17], I.Kronkvist[24], Z.Krumstein[16], W.Krupinski[18], P.Kubinec[7], W.Kucewicz[18], K.Kurvinen[15], C.Lacasta[49], I.Laktineh[25], S.Lamblot[23], J.W.Lamsa[1], L.Lanceri[46], D.W.Lane[1], P.Langefeld[52], I.Last[22], J-P.Laugier[39], R.Lauhakangas[15], G.Leder[50], F.Ledroit[14], V.Lefebure[2], C.K.Legan[1], R.Leitner[30], Y.Lemoigne[39], J.Lemonne[2], G.Lenzen[52], V.Lepeltier[19], T.Lesiak[36], D.Liko[50], R.Lindner[52], A.Lipniacka[36], I.Lippi[36], B.Loerstad[24], J.G.Loken[35], J.M.Lopez[41], D.Loukas[11], P.Lutz[39], L.Lyons[35], J.MacNaughton[50], G.Maehlum[17], A.Maio[21], V.Malychev[16], F.Mandl[50], J.Marco[41], R.Marco[41], B.Marechal[47], M.Margoni[36], J-C.Marin[9], C.Mariotti[40], A.Markou[11], T.Maron[52], C.Martinez-Rivero[41], F.Martinez-Vidal[49], S.Marti i Garcia[49], J.Masik[30], F.Matorras[41], C.Matteuzzi[9], G.Matthiae[38], M.Mazzucato[36], M.Mc Cubbin[9], R.Mc Kay[1], R.Mc Nulty[22], J.Medbo[48], M.Merk[31], C.Meroni[28], S.Meyer[17], W.T.Meyer[1], A.Miagkov[42], M.Michelotto[36], E.Migliore[45], L.Mirabito[25], W.A.Mitaroff[50], U.Mjoernmark[24], T.Moa[44], R.Moeller[29], K.Moenig[9], M.R.Monge[13], P.Morettini[13], H.Mueller[17], L.M.Mundim[6], W.J.Murray[37], B.Muryn[18], G.Myatt[35], F.Naraghi[14], F.L.Navarria[5], S.Navas[49], K.Nawrocki[51], P.Negri[28], W.Neumann[52], N.Neumeister[50], R.Nicolaidou[3], B.S.Nielsen[29], M.Nieuwenhuizen[31], V.Nikolaenko[10], P.Niss[44], A.Nomerotski[36], A.Normand[35], W.Oberschulte-Beckmann[17], V.Obraztsov[42], A.G.Olshevski[16], A.Onofre[21], R.Orava[15], K.Osterberg[15], A.Ouraou[39], P.Paganini[19], M.Paganoni[9], P.Pages[10], H.Palka[18], Th.D.Papadopoulou[32], K.Papageorgiou[11], L.Pape[9], C.Parkes[35], F.Parodi[13], A.Passeri[40], M.Pegoraro[36], L.Peralta[21], H.Pernegger[50], M.Pernicka[50], A.Perrotta[5], C.Petridou[46], A.Petrolini[13], M.Petrovyck[28,53], H.T.Phillips[37], G.Piana[13], F.Pierre[39], M.Pimenta[21], M.Pindo[28], S.Plaszczynski[19], O.Podobrin[17], M.E.Pol[6], G.Polok[18], P.Poropat[46], V.Pozdniakov[16], M.Prest[46], P.Privitera[38], N.Pukhaeva[16], A.Pullia[28], D.Radojicic[35], S.Ragazzi[28], H.Rahmani[32], J.Rames[12], P.N.Ratoff[20], A.L.Read[33], M.Reale[52], P.Rebecchi[19], N.G.Redaelli[28], M.Regler[50], D.Reid[9], P.B.Renton[35], L.K.Resvanis[3], F.Richard[19], J.Richardson[22], J.Ridky[12], G.Rinaudo[45], I.Ripp[39], A.Romero[45], I.Roncagliolo[13], P.Ronchese[36], L.Roos[14], E.I.Rosenberg[1], E.Rosso[9], P.Roudeau[19], T.Rovelli[5], W.Ruckstuhl[31], V.Ruhlmann-Kleider[39], A.Ruiz[41], H.Saarikko[15], Y.Sacquin[39], A.Sadovsky[16], G.Sajot[14], J.Salt[49], J.Sanchez[26], M.Sannino[13], M.Schimmelpfennig[17], H.Schneider[17], U.Schwickerath[17], M.A.E.Schyns[52], G.Sciolla[45], F.Scuri[46], P.Seager[20], Y.Sedykh[16], A.M.Segar[35], A.Seitz[17], R.Sekulin[37], R.C.Shellard[6], I.Siccama[31], P.Siegrist[39], S.Simonetti[39], F.Simonetto[36], A.N.Sisakian[16], B.Sitar[7], T.B.Skaali[33], G.Smadja[25], N.Smirnov[42], O.Smirnova[16], G.R.Smith[37], O.Solovianov[42], R.Sosnowski[51], D.Souza-Santos[6], T.Spassov[21], E.Spiriti[40], P.Sponholz[52], S.Squarcia[13], C.Stanescu[40], S.Stapnes[33], I.Stavitski[36], F.Stichelbaut[9], A.Stocchi[19], J.Strauss[50], R.Strub[10], B.Stugu[4], M.Szczekowski[51], M.Szeptycka[51], T.Tabarelli[28],

J.P.Tavernet[23], O.Tchikilev[42], A.Tilquin[27], J.Timmermans[31], L.G.Tkatchev[16], T.Todorov[10], D.Z.Toet[31], A.Tomaradze[2], B.Tome[21], A.Tonazzo[28], L.Tortora[40], G.Transtromer[24], D.Treille[9], W.Trischuk[9], G.Tristram[8], A.Trombini[19], C.Troncon[28], A.Tsirou[9], M-L.Turluer[39], I.A.Tyapkin[16], M.Tyndel[37], S.Tzamarias[22], B.Ueberschaer[52], O.Ullaland[9], V.Uvarov[42], G.Valenti[5], E.Vallazza[9], C.Vander Velde[2], G.W.Van Apeldoorn[31], P.Van Dam[31], W.K.Van Doninck[2], J.Van Eldik[31], N.Vassilopoulos[35], G.Vegni[28], L.Ventura[36], W.Venus[37], F.Verbeure[2], M.Verlato[36], L.S.Vertogradov[16], D.Vilanova[39], P.Vincent[25], L.Vitale[46], E.Vlasov[42], A.S.Vodopyanov[16], V.Vrba[12], H.Wahlen[52], C.Walck[44], F.Waldner[46], M.Weierstall[52], P.Weilhammer[9], C.Weiser[17], A.M.Wetherell[9], D.Wicke[52], J.H.Wickens[2], M.Wielers[17], G.R.Wilkinson[35], W.S.C.Williams[35], M.Winter[10], K.Woschnagg[48], K.Yip[35], O.Yushchenko[42], F.Zach[25], A.Zaitsev[42], A.Zalewska[18], P.Zalewski[51], D.Zavrtanik[43], E.Zevgolatakos[11], N.I.Zimin[16], M.Zito[39], D.Zontar[43], R.Zuberi[35], G.C.Zucchelli[44], G.Zumerle[36]

[1] Ames Laboratory and Department of Physics, Iowa State University, Ames IA 50011, USA
[2] Physics Department, Univ. Instelling Antwerpen, Universiteitsplein 1, B-2610 Wilrijk, Belgium
and IIHE, ULB-VUB, Pleinlaan 2, B-1050 Brussels, Belgium
and Faculté des Sciences, Univ. de l'Etat Mons, Av. Maistriau 19, B-7000 Mons, Belgium
[3] Physics Laboratory, University of Athens, Solonos Str. 104, GR-10680 Athens, Greece
[4] Department of Physics, University of Bergen, Allégaten 55, N-5007 Bergen, Norway
[5] Dipartimento di Fisica, Università di Bologna and INFN, Via Irnerio 46, I-40126 Bologna, Italy
[6] Centro Brasileiro de Pesquisas Físicas, rua Xavier Sigaud 150, RJ-22290 Rio de Janeiro, Brazil
and Depto. de Física, Pont. Univ. Católica, C.P. 38071 RJ-22453 Rio de Janeiro, Brazil
and Inst. de Física, Univ. Estadual do Rio de Janeiro, rua São Francisco Xavier 524, Rio de Janeiro, Brazil
[7] Comenius University, Faculty of Mathematics and Physics, Mlynska Dolina, SK-84215 Bratislava, Slovakia
[8] Collège de France, Lab. de Physique Corpusculaire, IN2P3-CNRS, F-75231 Paris Cedex 05, France
[9] CERN, CH-1211 Geneva 23, Switzerland
[10] Centre de Recherche Nucléaire, IN2P3 - CNRS/ULP - BP20, F-67037 Strasbourg Cedex, France
[11] Institute of Nuclear Physics, N.C.S.R. Demokritos, P.O. Box 60228, GR-15310 Athens, Greece
[12] FZU, Inst. of Physics of the C.A.S. High Energy Physics Division, Na Slovance 2, 180 40, Praha 8, Czech Republic
[13] Dipartimento di Fisica, Università di Genova and INFN, Via Dodecaneso 33, I-16146 Genova, Italy
[14] Institut des Sciences Nucléaires, IN2P3-CNRS, Université de Grenoble 1, F-38026 Grenoble Cedex, France
[15] Research Institute for High Energy Physics, SEFT, P.O. Box 9, FIN-00014 Helsinki, Finland
[16] Joint Institute for Nuclear Research, Dubna, Head Post Office, P.O. Box 79, 101 000 Moscow, Russian Federation
[17] Institut für Experimentelle Kernphysik, Universität Karlsruhe, Postfach 6980, D-76128 Karlsruhe, Germany
[18] Institute of Nuclear Physics and University of Mining and Metalurgy, Ul. Kawiory 26a, PL-30055 Krakow, Poland
[19] Université de Paris-Sud, Lab. de l'Accélérateur Linéaire, IN2P3-CNRS, Bât. 200, F-91405 Orsay Cedex, France
[20] School of Physics and Materials, University of Lancaster, Lancaster LA1 4YB, UK
[21] LIP, IST, FCUL - Av. Elias Garcia, 14-1^{o}, P-1000 Lisboa Codex, Portugal
[22] Department of Physics, University of Liverpool, P.O. Box 147, Liverpool L69 3BX, UK
[23] LPNHE, IN2P3-CNRS, Universités Paris VI et VII, Tour 33 (RdC), 4 place Jussieu, F-75252 Paris Cedex 05, France
[24] Department of Physics, University of Lund, Sölvegatan 14, S-22363 Lund, Sweden
[25] Université Claude Bernard de Lyon, IPNL, IN2P3-CNRS, F-69622 Villeurbanne Cedex, France
[26] Universidad Complutense, Avda. Complutense s/n, E-28040 Madrid, Spain
[27] Univ. d'Aix - Marseille II - CPP, IN2P3-CNRS, F-13288 Marseille Cedex 09, France
[28] Dipartimento di Fisica, Università di Milano and INFN, Via Celoria 16, I-20133 Milan, Italy
[29] Niels Bohr Institute, Blegdamsvej 17, DK-2100 Copenhagen 0, Denmark
[30] NC, Nuclear Centre of MFF, Charles University, Areal MFF, V Holesovickach 2, 180 00, Praha 8, Czech Republic
[31] NIKHEF-H, Postbus 41882, NL-1009 DB Amsterdam, The Netherlands
[32] National Technical University, Physics Department, Zografou Campus, GR-15773 Athens, Greece
[33] Physics Department, University of Oslo, Blindern, N-1000 Oslo 3, Norway
[34] Dpto. Fisica, Univ. Oviedo, C/P. Pérez Casas, S/N-33006 Oviedo, Spain
[35] Department of Physics, University of Oxford, Keble Road, Oxford OX1 3RH, UK
[36] Dipartimento di Fisica, Università di Padova and INFN, Via Marzolo 8, I-35131 Padua, Italy
[37] Rutherford Appleton Laboratory, Chilton, Didcot OX11 OQX, UK
[38] Dipartimento di Fisica, Università di Roma II and INFN, Tor Vergata, I-00173 Rome, Italy
[39] Centre d'Etudes de Saclay, DSM/DAPNIA, F-91191 Gif-sur-Yvette Cedex, France
[40] Istituto Superiore di Sanità, Ist. Naz. di Fisica Nucl. (INFN), Viale Regina Elena 299, I-00161 Rome, Italy
[41] Instituto de Fisica de Cantabria (CSIC-UC), Avda. los Castros, S/N-39006 Santander, Spain, (CICYT-AEN93-0832)
[42] Inst. for High Energy Physics, Serpukov P.O. Box 35, Protvino, (Moscow Region), Russian Federation
[43] J. Stefan Institute and Department of Physics, University of Ljubljana, Jamova 39, SI-61000 Ljubljana, Slovenia
[44] Fysikum, Stockholm University, Box 6730, S-113 85 Stockholm, Sweden
[45] Dipartimento di Fisica Sperimentale, Università di Torino and INFN, Via P. Giuria 1, I-10125 Turin, Italy
[46] Dipartimento di Fisica, Università di Trieste and INFN, Via A. Valerio 2, I-34127 Trieste, Italy
and Istituto di Fisica, Università di Udine, I-33100 Udine, Italy
[47] Univ. Federal do Rio de Janeiro, C.P. 68528 Cidade Univ., Ilha do Fundão BR-21945-970 Rio de Janeiro, Brazil
[48] Department of Radiation Sciences, University of Uppsala, P.O. Box 535, S-751 21 Uppsala, Sweden
[49] IFIC, Valencia-CSIC, and D.F.A.M.N., U. de Valencia, Avda. Dr. Moliner 50, E-46100 Burjassot (Valencia), Spain
[50] Institut für Hochenergiephysik, Österr. Akad. d. Wissensch., Nikolsdorfergasse 18, A-1050 Vienna, Austria
[51] Inst. Nuclear Studies and University of Warsaw, Ul. Hoza 69, PL-00681 Warsaw, Poland
[52] Fachbereich Physik, University of Wuppertal, Postfach 100 127, D-42097 Wuppertal 1, Germany
[53] On leave of absence from IHEP Serpukhov

1 Introduction

In the Standard Model, the $B_q^0 - \bar{B}_q^0$ ($q = d, s$) mixing is a direct consequence of second order weak interactions. Starting with a B_q^0 meson produced at time $t = 0$, the probability, $\mathcal{P}$, to observe a B_q^0 decaying at the time t can be written, neglecting effects from CP violation:

$$\mathcal{P}(B_q^0 \to B_q^0) \;=\; \tfrac{\Gamma_q}{2} e^{-\Gamma_q t}(\cosh(\tfrac{\Delta\Gamma_q}{2}t) \;+\; \cos(\Delta m_q t))$$

where $\Gamma_q = \frac{\Gamma_q^H + \Gamma_q^L}{2}$, $\Delta\Gamma_q = \Gamma_q^L - \Gamma_q^H$, $\Delta m_q = m_q^L - m_q^H$, and L and H denote respectively the light and heavy physical states. The oscillation period gives a direct measurement of the mass difference between the two physical states.

For B_d^0 mesons, the Standard Model predicts [1] that $\Delta\Gamma_d \ll \Delta m_d$. Therefore the previous expression simplifies to:

$$\mathcal{P}(B_d^0 \to B_d^0) \;=\; \Gamma_d e^{-\Gamma_d t} \cos^2(\tfrac{\Delta m_d t}{2})$$

and similarly:

$$\mathcal{P}(B_d^0 \to \overline{B_d^0}) \;=\; \Gamma_d e^{-\Gamma_d t} \sin^2(\tfrac{\Delta m_d t}{2})\,.$$

The time integrated mixing probability for B_d^0 mesons, $\chi_d = x_d^2 \;/\; [\; 2(1 + x_d^2)\;]$ with $x_d = \Delta m_d/\Gamma_d$, has been measured at the $\Upsilon(4S)$. An average time integrated mixing probability has been measured at LEP, namely $\bar{\chi} = f_d\chi_d + f_s\chi_s$, where f_d and f_s are the fractions of B_d^0 and B_s^0 mesons respectively in a b jet [2]. Time dependent oscillations of B_d^0 mesons have also been measured at LEP [3].

The analysis presented here gives a measurement of Δm_d based on data taken by DELPHI at LEP1 from 1991 to 1993. The principle of the method is the following: after having divided the charged and neutral particles from Z^0 decay into two hemispheres separated by the plane transverse to the sphericity axis, a "production sign" is defined on one side, which is correlated to the sign of the initial quark at the production point; in the other hemisphere the flight distance of the B hadron is evaluated and a "decay sign" is defined, correlated to the $B^0/\overline{B^0}$ nature of the decaying hadron. Three tagging procedures have been used, which give a measurement of the charge of the b or $\overline{b}$ quark when it decays inside the B hadron:

- Direct semileptonic decays of b quarks produce a negative lepton, with a branching fraction close to 10% per each lepton flavour. These leptons have usually a larger transverse momentum, relative to the axis of the jet they belong to, than those produced in lighter flavour decays.
- The dominant decay chain $b \to c \to s$ generates an excess of K^- relative to K^+ in B hadron decays (apart for $\overline{B_s^0}$ mesons for which similar numbers of kaons of the two signs are expected). Kaons from B hadron decays can be isolated by requiring that their measured trajectory has a significant offset relative to the position of the Z^0 decay.
- Finally the value of the mean charge of particles produced in a jet is sensitive to the charge of the b quark producing the jet.

In section 2 the components of the DELPHI detector which are important for this analysis are described. Section 3 presents the event selection, particle identification and Monte-Carlo simulation. In section 4 a measurement of Δm_d is obtained from the dilepton event sample alone. In section 5 the analysis is extended to other tagging procedures and conclusions are given in section 6. As the extended analysis includes most of the dilepton sample, only this last measurement has been quoted as the final result.

2 The DELPHI detector

The events used in this analysis were collected at LEP running near the Z^0 peak with the DELPHI detector [4]. The performance of the detector is detailed in [5]. The relevant parts for lepton identification are the muon chambers and the electromagnetic calorimeters. The Vertex Detector is used in combination with the central tracking devices to measure precisely the charged particle trajectories close to the beam interaction point.

The DELPHI reference frame is defined with z along the e^- beam, x towards the centre of LEP and y upwards. Angular coordinates are θ, measured from the z axis, and the azimuth, ϕ, measured from the xz plane, while R is the radial distance from the z axis.

The muon chambers are drift chambers located at the periphery of DELPHI. The barrel part ($-0.63 < cos(\theta) < 0.63$) is composed of three sets of modules, each of two active layers, and gives z and $R\phi$ coordinates. In the forward part, two layers of two planes give the x and y coordinates in the transverse plane. The precision of these detectors has to be taken into account for muon identification: it has been measured to be ± 1 cm in z and ± 0.2 cm in $R\phi$ for the barrel part, and ± 0.4 cm for each of the two coordinates given by the forward part. The number of absorption lengths determines the hadron contamination and is approximatively 8 at 90°.

Electrons are absorbed in the electromagnetic calorimeters; the High density Projection Chamber (HPC) covers the barrel part and provides three dimensional information on electromagnetic showers with 18 radiation lengths thickness. Calorimeters in the end-cap regions are not used in this analysis because their acceptance is not matched with the solid angle covered by the vertex detector.

During the relevant period of data taking (1991 to 1993), the Vertex Detector (VD) [6] consisted of three cylinders of silicon strip detectors, at average radii of 6.3, 9 and 11 cm. This detector measured the coordinates of charged particle tracks in the transverse plane with respect to the beam direction with a precision of $\pm 8\mu$m. The association of this detector to the central tracking system of DELPHI, consisting of the Time Projection Chamber (TPC) and the Inner and Outer Detectors, gave a $\sqrt{24^2 + (69/p)^2}$ μm (p in GeV/c units) precision on the impact parameter of charged particles with respect to the primary vertex. The 192 sense wires of the TPC also measure the specific energy loss, or dE/dx, of charged particles, as the 80% truncated mean of the amplitudes of the wire signals, with a minimum requirement of 30 wires. This dE/dx measurement is available for 75% of charged particles in hadronic jets, with an average precision of $\pm 7.5\%$.

Charged hadron identification uses the RICH detectors. These consist of two parts: a liquid radiator and a gas radiator. With sufficiently tight cuts, the liquid radiator can provide complete $p/\mathrm{K}/\pi$ separation in the momentum range 2.5 – 8 GeV/c by measuring the Cherenkov angle with high precision [5]. In this momentum range, the gas radiator operates in the "veto" mode (kaons and protons give no Cherenkov photons and are thus distinguished from pions and leptons, but not from each other). But in the range 8 – 20 GeV/c it can again distinguish kaons from all other charged particles by measuring the radius of the ring of detected Cherenkov photons. A complete description of the RICH detector is given in [7].

3 Event Selection

Hadronic decays of the Z^0 were selected by requiring the total energy of the charged particles in each hemisphere to exceed 3 GeV (assuming all charged particles to be pions), the total energy of the charged particles to exceed 15 GeV and at least 5 charged particles with momenta above 0.2 GeV/c. For the dilepton analysis, the detectors needed for lepton identification were required to be operational. These requirements gave 204000 events in 1991, 589000 in 1992 and 572000 in 1993 with an efficiency ranging between 81% and 85%. For the second analysis, the event thrust axis was required to be well within the acceptance of the Vertex Detector and the RICH through the condition $45° < \theta_{thrust} < 135°$. This selected 458000 events in 1992 and 457000 in 1993 (the RICH information was available in 2/3 of this sample), and 930000 events were kept in the simulated sample.

Simulated events have been generated using the JETSET parton shower model [8] and including the full detector simulation [9]. The parameters in this simulation have been adjusted from previous studies [10]. The B hadron semileptonic decays have been simulated using the model of ISGW [12] with a fraction of 30% for D^{**} production. Weights were applied to the simulated events to effectively update the main B decay parameters used in the event generation to current values, as summarized in Table 1 [11].

Parameter	value in simulation	value applied
B_d lifetime	1.60 ps	1.57 ps
B_s lifetime	1.60 ps	1.58 ps
B^+ lifetime	1.60 ps	1.63 ps
b-baryons lifetime	1.60 ps	1.18 ps
$Br(b \to \ell)$	0.11	0.11
$Br(b \to c \to \overline{\ell})$	0.081	0.081
$Br(b \to \overline{c} \to l)$	0.008	0.008
χ_s	0.5	0.5

Table 1: *Main B decay parameters used in generating the simulated events and the effective values applied in the analysis by reweighting the events.*

Each selected event is divided into two hemispheres separated by the plane transverse to the sphericity axis. A clustering analysis based on the JETSET algorithm LUCLUS with default parameters is used to define jets using both charged and neutral particles [8]. These jets are used to compute the p_t of each particle of the event, as the transverse momentum of this particle with respect to the axis of the jet it belongs to, after having removed this particle from its jet.

3.1 Lepton identification

A minimum momentum of 3 GeV/c is required for muons and electrons.

Muon chamber information is associated to the information coming from the central tracking devices of DELPHI to identify muons in the regions $53° < \theta < 127°$ (barrel part) and $20° < \theta < 42°$, $138° < \theta < 160°$ (forward part) [5].

The identification of electrons is performed using information coming from the HPC in the region $45° < \theta < 135°$, and the ionization measured in the Time Projection Chamber. Electrons from photon conversion are rejected. The global identification efficiencies for muons and electrons, in the selected momentum range and within the angular acceptances of the muon chambers and HPC respectively, are given in Table 2, together with the corresponding probabilities for a hadron to be misidentified as a lepton. These values have been obtained using the detailed simulation code of the DELPHI detector, DELSIM [5], and have been checked on real data using selected events samples such as $\mathrm{K}^0_s \to \pi^+\pi^-$, $\mathrm{Z}^0 \to \mu^+\mu^-$, converted photons before the HPC, $\gamma\gamma \to \ell^+\ell^-$ and hadronic τ decays [13].

	$\mathcal{P}(\ell \to \ell)\%$	$\mathcal{P}(h \to \ell)\%$
muon	86.	0.7
electron	60.	0.4

Table 2: *Mean values of lepton identification probabilities for real leptons and for hadrons, with momenta larger than 3 GeV/c and in the angular regions defined in the text.*

3.2 Kaon identification

Charged kaons are identified in the RICH using the standard DELPHI algorithm [5]. In 1993, data from the liquid radiator are available for only small fraction of the total time. Therefore, for uniformity, only data from the gas radiator are used in this analysis. The identification efficiencies are momentum dependent. They were evaluated from the simulation and verified using pure subsamples from K^0, Λ and ϕ decays. Only kaons with momentum above 3 GeV/c were used in the analysis. With the loose cuts that were applied, the probability of a $\mathrm{K}^\pm$ within the angular acceptance of the barrel RICH being identified correctly is about 65% for $3 < p < 8.5$ GeV/c and 80% for $8.5 < p < 15$ GeV/c. That for a proton to be seen as a kaon also averages 65% in the veto region, $3 < p < 8.5$ GeV/c, where only lighter particles give Cherenkov light, falling to average 26% for $8.5 < p < 15$ GeV/c. The probability for a pion to be seen as a kaon is around 8%.

4 Measurement of Δm_d from the dilepton sample

The dilepton sample is considered first because this is the simplest channel to select and results can be compared with similar analyses performed in other experiments [3].

Both muons and electrons are selected with a p_t larger than 1 GeV/c. If several leptons are found in a given hemisphere, only the one with the highest p_t is kept. The p_t cut dependence of the final result will be considered as a possible systematic uncertainty. Each lepton is considered in turn to extract time information and its charge is compared with the charge of the lepton in the opposite hemisphere, to tag the oscillation. The lepton containing time information is required to be associated to at least two hits in different layers of the Vertex Detector (VD), while there is no requirement of VD information

for the other lepton. As a result, each Z^0 decay containing two leptons in opposite hemispheres may lead to one or two time measurement(s).

In real data, the selected dilepton sample yields 1073 time measurements associated with a same sign correlation, and 2151 associated with an opposite sign correlation. 2055 muons and 1169 electrons are selected on the measurement side, and the tagging side sample contains 2057 muons plus 1167 electrons. The efficiency of the VD selection has been found to be $88 \pm 1\%$ for muons and $82 \pm 1\%$ for electrons.

The composition of the total sample expected from the simulation (all sign combinations mixed together) is given in Table 3. The main component is from direct b semileptonic decays. The fraction of cascade ($b \to c \to \overline{\ell}$) decays is of the order of 10% and the fraction of charm events remains small. The cut at 1 GeV/c on the lepton transverse momentum has been optimized knowing that the signal from oscillations depends on the difference between the fractions of direct and cascade semileptonic decays, and on the number of selected events. The remaining events contain the following categories, with small associated fractions: semileptonic decays in a b decay chain, fake leptons in a b decay chain, charged particles coming from the primary vertex in $b\overline{b}$ events and light quark events.

Lepton origin	Relative fraction
$b \to \ell$	79.4%
$b \to c \to \overline{\ell}$	9.6%
other leptons in a b decay chain	3.0%
fake leptons in a b decay chain	2.7%
primary vertex particles in a b hemisphere	1.5%
$c \to \overline{\ell}$ lepton	3.3%
$u,\ d,\ s \to$ lepton	0.5%

Table 3: *Composition of the simulated sample on the impact parameter measurement side.*

4.1 Measurement of the B decay time using the lepton impact parameter

The measurement of Δm_d is extracted from a study of the impact parameter distribution obtained from same sign and opposite sign dilepton events.

To determine the impact parameter, a primary vertex is first reconstructed in the transverse ($R\phi$) plane for each event, through an iterative vertex fit including the beam profile information [14,5], where at each step the track contributing most to the χ^2 is removed until none contributes more than 5 χ^2 units. The impact parameter δ of the lepton is then measured with respect to the primary vertex position and has a positive or negative lifetime sign depending on the relative position of the primary vertex and the intersection of the lepton with the jet along the jet direction. $t_\delta = \delta/c$ is the time sensitive variable which is used in the analysis. The precision on the impact parameter is

dominated by the accuracy on the primary vertex determination (approximately $\pm 50\mu$m in the horizontal and $\pm 20\mu$m in the vertical direction).

The correlation between t_δ and the true proper time of the B meson is smeared by the decay kinematics and by the energy distribution of B mesons. The effective proper time resolution $(t_\delta - t_B^{true})/t_B^{true}$ has a width of 70% and a 40% shift towards lower values due to the reconstruction procedure which is performed in the transverse plane only; such a resolution is in fact sufficient to study the slow B_d^0 oscillation.

The data and simulated samples are composed of events with one t_δ measurement in a single hemisphere, and of events with t_δ measurements in both hemispheres. The data sample contains 249 same sign and 455 opposite sign events with one measurement, 412 same sign and 848 opposite sign events with two measurements. When Δm_d is set to 0.45 ps^{-1} in the simulation, the simulated sample contains 752 same sign and 1418 opposite sign events with one measurement, and 1407 same sign and 3032 opposite sign events with two measurements.

4.2 Fitting method and results

The t_δ distribution obtained from same sign events has been divided by the t_δ distribution obtained using opposite sign events, and the resulting distribution will be referred to as the $R_{++/+-}(t_\delta)$ distribution (Figure 1). Each t_δ measurement enters once in this distribution. In the absence of B_d^0 oscillations, the distribution is expected to be flat at large t_δ; the observed time dependence comes from B_d^0 oscillations.

The $R_{++/+-}$ distributions obtained from the data and from the simulation have been compared using a binned χ^2 fit with Δm_d as the only free parameter. For a given Δm_d in the fit the simulated data have been adjusted to conform to the probabilities given in the introduction. Events with one and two time measurements have been treated separately in the fit. For events with two measurements, the two-dimensional distributions $R_{++/+-}(t_{\delta 1}, t_{\delta 2})$ have been compared. The binning used in this fit and in the following has been defined such that each bin or each box contains at least 10 events. To satisfy this condition, 3 bins were used for events with a single t_δ measurement (grouping the last 3 bins of Figure 1 together), and a 3×3 grid was used for events with two measurements. The Δm_d measurement obtained in this way is

$$\Delta m_d = 0.47 \pm 0.08\,\mathrm{ps}^{-1}$$

and the corresponding χ^2 value is found to be 7.5 for 11 degrees of freedom.

Figure 2 shows the fraction of same sign correlations, F_{++}, corresponding to the final Δm_d measurement. This representation shows the different components of the same sign sample, listed in Table 4. The direct $b \to l$ contribution is close to 50% because the oscillation may have occurred in the opposite (tagging) hemisphere. The amounts of mixed B_d^0 and mixed B_s^0 in the same sign sample are similar, as expected since $f_d \chi_d$ is known to be roughly equal to $f_s \chi_s$. Since cascade decays fake mixed B^0 decays, there is a large contribution from $b \to c \to \bar{l}$ events. The contributions from other categories of events are small: $b \to$ fake lepton, $b \to X \to l$ decay chains, primary vertex particles in $b\bar{b}$ events, and light quark ($udsc$) events (roughly one third of the 7.8% quoted in Table 4 for each of these last three categories). It can be seen from Figure 2 that the time evolution is due to mixed B_d^0 events, the behaviour of the other components being time-independent.

Event type	fraction
$\overline{\mathrm{B}^0_d} \to \mathrm{B}^0_d \to \overline{l}$	0.121
$\overline{\mathrm{B}^0_s} \to \mathrm{B}^0_s \to \overline{l}$	0.105
$b \to c \to \overline{l}$	0.209
$unmixed\ \overline{\mathrm{B}^0},\ \mathrm{B}^{\pm},\ \Lambda_b \to l$	0.455
$b \to fake\ l$	0.032
others	0.078

Table 4: *Composition of the same sign sample on the t_δ measurement side.*

4.3 Study of systematic uncertainties

The systematic uncertainties are computed by varying all the relevant parameters of the simulation in turn and re-making the Δm_d fit each time. Four dominant effects have been studied (see Table 5):

- B hadron lifetimes: the largest contribution comes from the uncertainty on the B^0_d lifetime.
- B hadron production rates: the fractions f_d and f_s of B^0_d and B^0_s mesons produced in the fragmentation of a b quark have been obtained from the measurements of the integrated oscillation rates $\overline{\chi}$ and χ_d obtained at LEP, by other experiments and at the $\Upsilon(4S)$ [15]. The fraction of b-baryon production, $f_{b-baryon} = (11.6 \pm 3.2\%)$ has been taken from measurements of Λ_c production in c jets [16], assuming that it is similar for Λ_b in b jets and using a rate of $(2 \pm 2\%)$ for Ξ_b states. From the expressions:

  $$1 = f_d + f_u + f_s + f_{b-baryon} \text{ and } \overline{\chi} = f_d\chi_d + f_s\chi_s$$

  and assuming $f_d = f_u$ because, for B mesons, as opposed to D mesons, no asymmetry between the B^0_d and B^- production rates is expected from the decay of excited states, one obtains:

  $$f_d = \frac{(1-f_{b-baryon})\chi_s - \overline{\chi}}{2\chi_s - \chi_d} \text{ and } f_s = \frac{2\overline{\chi} - (1-f_{b-baryon})\chi_d}{2\chi_s - \chi_d}.$$

  Using $\chi_s = 0.5$, $\overline{\chi} = 0.116 \pm 0.006$, and $\chi_d = 0.168 \pm 0.016$, one obtains $f_d = (39.2 \pm 2.2\%)$ and $f_s = (10.0 \pm 2.2\%)$. The uncertainties on f_d and on f_s appear to be only weakly correlated. The error on f_d is dominated by the uncertainty on $f_{b-baryon}$ and the error on f_s receives similar contributions from the errors on $\overline{\chi}$ and on χ_d. As a consequence, in the following, it has been assumed that f_d and f_s vary independently and that their corresponding variation is compensated by a change in $f_{b-baryon}$.
- Lepton origin: uncertainties on direct and cascade branching fractions remain the second source of uncertainty after the effect from f_d/f_s. Uncertainties on direct and cascade semileptonic branching fractions have been treated independently and the quoted values include the additional uncertainties coming from the modelling of the decays.
- Finally, χ_s is varied separately, and the corresponding variation on Δm_d is 0.015 ps^{-1}.

Parameter	Central value	Uncertainty	Effect on Δm_d (ps^{-1})
B_d lifetime	1.57 ps	$\pm$ 0.05 ps	$\mp$ 0.012
global b lifetime	1.567 ps	$\pm$ 0.020 ps	$\mp$ 0.003
f_d	0.392	$\pm$ 0.022	$\mp$ 0.010
f_s	0.100	$\pm$ 0.022	$\mp$ 0.045
$\mathrm{Br}(b \to l)$	0.110	$\pm$ 0.010	$\pm$ 0.050
$\mathrm{Br}(b \to c \to \overline{l})$	0.081	$\pm$ 0.008	$\mp$ 0.046
$c \to \overline{l}$ fraction	0.030	$\pm$ 0.003	$\pm$ 0.003
Background fraction	0.034	$\pm$ 0.007	$\mp$ 0.015
χ_s	0.50	-0.03	+0.015

Table 5: *Contributions to the systematic error on* Δm_d.

It has been checked that the contribution from the uncertainty on the b quark fragmentation distribution is negligible by fitting the simulated b fragmentation function with a Peterson function, and changing the ϵ parameter so that the mean fraction of the beam energy, taken by the B meson, varies between 0.68 and 0.72.

Performing the fit on the sample of events which give only one t_δ measurement leads to:

$$\Delta m_d = 0.46^{+0.15}_{-0.12}\ \mathrm{ps}^{-1}\ ,$$

and using only events with two t_δ measurements gives:

$$\Delta m_d = 0.47^{+0.11}_{-0.10}\ \mathrm{ps}^{-1}\ .$$

It has also been checked that the results found using muons or electrons only, as well as 1992 or 1993 data only, were compatible within the statistical errors. Because of the limited statistics, these last checks were done using a global one-dimensional fit to the $R_{++/+-}(t_\delta)$ distribution with each t_δ measurement entering once.

Finally, the p_t cut was varied (keeping the same momentum cuts). No systematic effect was observed (Figure 3). The cut $p_t > 1$ GeV/c gave the smallest total error.

Adding in quadrature the contributions to the systematic error given in Table 5 yields the result:

$$\Delta m_d = 0.47 \pm 0.08\ (stat.)\ ^{+0.09}_{-0.08}\ (syst.)\ \mathrm{ps}^{-1}\ .$$

To separate the contributions to the fitted result coming from the time-averaged value of $R_{++/+-}$ and from its time dependence, a fit may be done with both a time-averaged mixing parameter $\bar{\chi} = f_d\chi_d + f_s\chi_s$ and a time-dependent parameter Δm_d^{freq} in a formulation modified so that Δm_d^{freq} gives zero contribution to the time-averaged value of $R_{++/+-}$ and the two fitted values are therefore uncorrelated. Such a fit gives

$$\Delta m_d^{freq} = 0.74\ ^{+0.17}_{-0.16}\ \pm 0.01\ \mathrm{ps}$$

and, expressing the $\bar{\chi}$ value thus obtained in terms of a frequency parameter Δm_d^{norm},

$$\Delta m_d^{norm} = 0.40 \pm 0.08\ ^{+0.09}_{-0.08}\ \mathrm{ps}$$

Comparing these two values it can be seen that, while most of the statistical weight in this measurement comes from the time-averaged value of $R_{++/+-}$, the time-dependence is also significant and is associated with a much smaller systematic uncertainty.

5 Measurement of Δm_d using leptons, $K^{\pm}$ and jet charge

In the following, the analysis of section 4 has been extended to include additional final states using identified charged kaons and the mean jet charge. The B decay distance will also be evaluated in space to enhance the sensitivity of the measurement to oscillations.

Tagging procedures used to define the samples of mixed and unmixed events candidates are described along with the algorithm used to measure the B hadron decay distance. The fitting procedure used to measure Δm_d is then given and the sources of systematic uncertainties are analyzed. The tagging probabilities and decay distance parametrizations have been evaluated for seven categories of hemispheres: u/d, s, c, $B^{\pm}$, B^0_d, B^0_s, b-baryons.

For each category and each tagging indicator the probabilities $\mathcal{P}^{right}_{tag}$ and $\mathcal{P}^{wrong}_{tag}$, to have a right sign or a wrong sign, have been obtained from simulation. They have been defined as "right" ("wrong") if the "production" sign is the same as (opposite to) the sign of the quark or of the antiquark emitted in the hemisphere, assuming that its flavour is always beauty. For B^0_d mesons these probabilities include the effect of the time-integrated oscillation: they have been computed for different values of Δm_d and the corresponding values are compatible with a linear interpolation. The B^0_s oscillation frequency is assumed to be high enough to give constant values, independent of the decay distance.

5.1 Tagging procedures

The measurements of the signs of three variables have been used, in a combined way, to establish the presence of a b or a $\overline{b}$ quark in a given hemisphere ("production" sign) and to identify a B or a $\overline{\mathrm{B}}$ meson when it decays ("decay" sign). These variables are:

- The *charge of leptons* emitted at p_t larger than 1 GeV/c. Lepton selection cuts are similar to those applied in section 4. If two particles of opposite sign fulfill these conditions, in the same hemisphere, the event is not kept. This "production" sign is defined in 9 % of the b hemispheres and the ratio right sign/wrong sign to correctly identify a b or a $\overline{b}$ quark is about 5.
- The *charge of kaons* produced at a secondary vertex. This tag is based on the dominant decay chain $b \to c \to s$ which implies that the sign of a secondary kaon is strongly correlated to the sign of the decaying quark. This has been studied in detail and measured in [17], and the fractions of decays with a right/wrong sign kaon (excluding ambiguous cases with a K^+ *and* a K^- in the same hemisphere) are roughly 50% and 10 % respectively. Kaons have been identified by the RICH detector in the range $3 < p < 15$ GeV/c. An additional cut is applied to favour a secondary $K^{\pm}$ from a B by requiring that its impact parameter with respect to the main vertex be larger than 1.5 times the measurement error. This production sign is defined in 23 % of cases, i.e. more frequently than the lepton sign, but the ratio right sign/wrong sign, of about 2, is lower. More background is also expected from u, d, s, c flavors.
- The *mean jet charge*, which is a weighted sum of the charges of particles belonging to the most energetic jet in the hemisphere. It depends on the charge of the quark producing this jet and is defined as:

$$Q_{jet} = (\sum q_i p_i^{\kappa})/(\sum p_i^{\kappa})$$

where, in the denominator, the sum is extended also to neutral particles. p_i and q_i are the individual particle momenta and charges. The weighting exponent κ is

chosen to be 0.6 to optimize the discrimination [18] (however its precise value is not crucial). The mean value of Q_{jet} is slightly biased by nuclear interactions in the detector: in practice the sign of $(Q_{jet} - 0.015)$ gives the right $b/\overline{b}$ nature in 62 % of the cases.
The b purity, which is the fraction of $b\overline{b}$ events in the selected sample, is improved by applying a b-tagging condition obtained from the values of the impact parameters, δ, of the n_t charged particles in the jet, relative to the event main vertex:

$$C_b \;=\; \frac{1}{n_t - 1} \sum_{i=1}^{n_t - 1} \frac{\delta_i^2}{\sigma_{\delta_i}^2} \;>\; 2.0$$

The track with the largest contribution has been excluded from the sum to reduce the effects of secondary interactions, decays, or poor measurements. Uncertainties on track impact parameters, σ_δ, include track measurement errors and uncertainties on the Z^0 decay point.

To optimize the discrimination and to reduce double counting, the "production" sign has been obtained using the following indicators for a hemisphere:

- *Jet sign* and *lepton sign* $(j + l)$ in agreement: this discriminates better than the lepton sign alone. This indicator is defined in 8% of the b hemispheres.
- *Jet sign* and *kaon sign* in agreement $(j + \mathrm{K})$: this indicator is defined in 16% of the b hemispheres.
- *Jet sign* alone with *b-tagging* condition $(j + b\ tag)$: this is used when the other criteria are not defined, provided $|Q_{jet} - 0.015| > 0.1$. This condition gives on average 67 % of right sign assignments and is defined for 39% of the b hemispheres.

The probabilities, per event hemisphere, of measuring a production sign have been obtained from the simulation and are given in Table 6.

To define the decay signs (see Table 7 discussed below), only the *lepton sign* and *kaon sign* have been used because the *jet sign* is not sensitive enough to the transformation of a B^0 into a $\overline{B^0}$ inside a jet. Leptons have been selected in the same way as before. For kaons, the condition on the impact parameter has been removed, in order not to bias the B meson flight distance distribution.

5.2 Measurement of the B decay distance

As seen above, where it was shown that even the impact parameter distribution could be used, because the $B_d^0 - \overline{B_d^0}$ oscillation period is large and the b quark fragmentation distribution is peaked at large values, it is not crucial to have a very accurate evaluation of the B decay time. The B decay distance distribution is more sensitive than the impact parameter distribution and has been used throughout this analysis.

The interaction point has been determined following the approach explained in section 4.1. To evaluate the B decay point, advantage was taken of the gathering of B decay products around the jet axis by selecting well-measured charged particles with at least 2 points associated in the Vertex Detector and situated within 25° of the thrust axis of the most energetic jet in the hemisphere. A "pseudo-secondary vertex" has been fitted using this set of particles, which is a mixture of primary and secondary particles, often including further decay products of a D coming from the B itself with probabilities that are independent of the B flight distance. In order to keep long flight distances, no cut has been applied on the χ^2 probability of this vertex. As a result, the expectation value, λ, of

Category	$\mathcal{P}_{tag}^{right}$ $(l+j)$ $\mathcal{P}_{tag}^{wrong}$ $(l+j)$	$\mathcal{P}_{tag}^{right}$ $(\mathrm{K}+j)$ $\mathcal{P}_{tag}^{wrong}$ $(\mathrm{K}+j)$	$\mathcal{P}_{tag}^{right}$ $(j+b\ tag)$ $\mathcal{P}_{tag}^{wrong}$ $(j+b\ tag)$
u/d	0.0072(01) 0.0044(01)	0.0247(02) 0.0152(02)	0.0500(03) 0.0305(02)
s	0.0075(02) 0.0025(01)	0.0387(04) 0.0166(02)	0.0495(04) 0.0279(03)
c	0.0041(01) 0.0170(03)	0.0577(05) 0.0364(04)	0.0740(06) 0.1025(07)
$\mathrm{B}^{\pm}$	0.0716(08) 0.0073(03)	0.1434(11) 0.0327(05)	0.2586(15) 0.1262(10)
B_d^0	0.0565(07) $-0.020\ \delta m$ 0.0214(04) $+\ 0.020\ \delta m$	0.1023(09) $-0.036\ \delta m$ 0.0520(06) $+\ 0.033\ \delta m$	0.2303(14) $-0.025\ \delta m$ 0.1620(12) $+\ 0.026\ \delta m$
B_s^0	0.0380(10) 0.0356(10)	0.0898(16) 0.0659(13)	0.2036(24) 0.1675(22)
b-baryons	0.0604(23) 0.0070(08)	0.0971(29) 0.0664(24)	0.1818(40) 0.1711(39)

Table 6: *Probabilities of right/wrong sign in the production hemisphere. For B_d^0, the quoted values correspond to $\Delta m_d = 0.50\ ps^{-1}$ and have a linear dependence on $\delta m = \Delta m_d - 0.50$. The numbers in parentheses are the 1-standard deviation statistical uncertainties only on the last digits.*

the distance from the primary vertex to this pseudo-secondary vertex depends linearly on the actual flight distance as shown in Figure 4. The tails in the distributions have been removed partially by a cut on the longitudinal error of the vertex fit. This procedure does not bias the decay distance distribution because it does not rely on the actual value of the χ^2 of the vertex fit. Figure 5 compares the normalized λ distribution for data and simulated events. An additional smearing of the simulated distribution has been performed by adding a random term distributed according to a Breit-Wigner function, with a half-width of 140μm, so that the two distributions agree for negative values of λ.

5.3 Parametrization and fitting procedure

The basic assumption is that the probabilities of correctly defining the production sign, the decay sign and the distance estimate are independent for a given flavour. As a consequence the two hemispheres can be parametrized separately but the different B hadrons have to be distinguished.

Let λ be the flight distance estimator and $\mathcal{P}_{cat}(\lambda)$ the probability density distribution to observe a given value of λ in a hemisphere for a given category. For b categories, the distribution $\mathcal{P}_{cat}(\lambda)$ is the convolution of the exponential b-decay time distribution with the b quark fragmentation function and with the resolution function on λ. As a result, it is difficult to write a reliable analytic expression for $\mathcal{P}_{cat}$. The simplest solution is to take this distribution from the simulation. Small values of λ are largely contaminated by the u, d, s, c background and in addition they contain very little information on the oscillation frequency, because they correspond to times where the $\sin^2(\Delta m_d t/2)$ factor is

small. For λ larger than 2 mm, the $\mathcal{P}_{cat}(\lambda)$ distributions are close to exponentials. Figure 6 shows how the slopes corresponding to different B hadrons, simulated with the same lifetime, exhibit slight differences due to the topological selection because the fractions of primary and secondary particles at the pseudo-secondary vertex are not exactly the same. For u/d and s categories, the shape of $\mathcal{P}_{cat}(\lambda)$ is dominated by the resolution (see Figure 7). For the c category, charm decays also give a significant contribution. The $\mathcal{P}_{cat}(\lambda)$ distributions have been parametrized using the exponential of a fourth order polynomial in the range $\lambda > 2$mm. These distributions have been normalized so that $\int_{\lambda_{min}}^{\infty} \mathcal{P}_{cat}(\lambda) \; = \; 1$.

As for the quark tagging procedures, at decay time the B meson can be signed correctly or not by the lepton or kaon charges and the corresponding probabilities ($\mathcal{P}_{dec,cat}^{right/wrong}$) have been evaluated for all values of λ larger than λ_{min}.

For charged B mesons or b-baryons the final probability density distribution to measure a decay distance λ is then:

$$\mathcal{P}_{dec,cat}^{right/wrong}(\lambda) = \mathcal{P}_{dec,cat}^{right/wrong} \; \mathcal{P}_{cat}(\lambda)\,.$$

For B_d^0 mesons these probabilities are different if they have oscillated ($\mathcal{P}_{dec,osc}^{right/wrong}$) or not ($\mathcal{P}_{dec,noosc}^{right/wrong}$) and have been evaluated separately. Table 7 shows that the right/wrong probabilities are not far from being simply exchanged when the B^0 has oscillated.

Then the distance-dependent probability may be written:

$$\mathcal{P}_{dec}^{right/wrong}(\lambda) = [\; \mathcal{P}_{dec,noosc}^{right/wrong} \; (1 - \mathcal{P}_{osc}(\lambda)) + \mathcal{P}_{dec,osc}^{right/wrong} \; \mathcal{P}_{osc}(\lambda) \;]\; \mathcal{P}_{B_d^0}(\lambda)$$

where $\mathcal{P}_{osc}(\lambda)$ is the probability, for a B_d^0 decaying at λ, to have oscillated. It has been parametrized by a polynomial of degree 4 or 5 in λ for 16 different values of Δm_d between 0.2 and 0.95 ps^{-1} (see Figure 8); a smoothed interpolation then gives its value at any Δm_d.

Finally one can define, for a given pair of hemispheres in a hadronic event, the probability to find a like/unlike sign correlation between them as a function of λ:

$$\mathcal{P}^{\;like\;sign}_{tag,dec}(\lambda) = \sum_{flav} R_{flav} \; [\; \mathcal{P}^{right}_{tag,flav} \; \mathcal{P}^{wrong}_{dec,flav}(\lambda) + \mathcal{P}^{wrong}_{tag,flav} \; \mathcal{P}^{right}_{dec,flav}(\lambda) \;]$$

$$\mathcal{P}^{\;unlike\;sign}_{tag,dec}(\lambda) = \sum_{flav} R_{flav} \; [\; \mathcal{P}^{right}_{tag,flav} \; \mathcal{P}^{right}_{dec,flav}(\lambda) + \mathcal{P}^{wrong}_{tag,flav} \; \mathcal{P}^{wrong}_{dec,flav}(\lambda) \;]\,,$$

where R_{flav} is the fraction of the corresponding flavour in hadronic events. For u/d, s, c flavours, the $\mathcal{P}_{flav}$ variables correspond to the $\mathcal{P}_{cat}$ previously defined; for the b flavour, $\mathcal{P}_{flav}$ is obtained by summing over the four B hadron categories, weighted by their respective fractions.

An unbinned maximum likelihood method is applied to the set of tagged events where λ is measured and greater than λ_{min} in order to fit the parameter Δm_d. The following function is minimised using the MINUIT [19] program:

$$\mathcal{L} = - \sum_{like\;sign\;evts} \ln(\mathcal{P}^{\;like\;sign}_{tag,dec}(\lambda, \Delta m_d)) \; - \sum_{unlike\;sign\;evts} \ln(\mathcal{P}^{\;unlike\;sign}_{tag,dec}(\lambda, \Delta m_d))\,.$$

The same procedure is applied to simulated events to check its consistency.

Category	$\mathcal{P}_{dec}^{right}$ (l) $\mathcal{P}_{dec}^{wrong}$ (l)	$\mathcal{P}_{dec}^{right}$ (K) $\mathcal{P}_{dec}^{wrong}$ (K)
u/d	0.0003(00) 0.0002(00)	0.0073(01) 0.0048(01)
s	0.0003(00) 0.0002(00)	0.0085(02) 0.0075(02)
c	0.0005(00) 0.0019(00)	0.0212(03) 0.0101(02)
$B^{\pm}$	0.0289(05) 0.0045(02)	0.0864(08) 0.0286(05)
B_d^0(no oscill.)	0.0274(05) 0.0068(02)	0.0784(08) 0.0282(05)
B_d^0(oscill.)	0.0081(03) 0.0262(05)	0.0291(05) 0.0775(08)
B_s^0	0.0165(07) 0.0161(07)	0.0608(13) 0.0489(12)
b-baryons	0.0245(14) 0.0025(05)	0.0614(22) 0.0465(20)

Table 7: *Probabilities of finding right/wrong production sign in the decay hemisphere after the 2mm flight distance cut. The numbers in parentheses are the 1-standard deviation statistical uncertainties on the last digits.*

5.4 Results and study of systematic errors

The fit has been performed on real data with $\lambda_{min} = 2$mm. Table 8 gives the number of entries available for each combination of sign indicators. The result, accounting for the effect of double entries, is:

$$\Delta m_d = 0.568^{+0.050}_{-0.046}\ (stat.)\ \mathrm{ps}^{-1}\ .$$

decay sign $\downarrow$ tag sign $\rightarrow$	$j+l$	$j+\mathrm{K}$	$j+b\ tag$
l	1383	1347	7350
K	2264	4494	12575

Table 8: *Number of entries for each sign combination with $\lambda > 2$ mm.*

The same procedure, applied on a simulated sample generated with $\Delta m_d = 0.50$ ps^{-1} and with similar statistics as the data, gives

$$\Delta m_d = 0.470 \pm 0.039\ \mathrm{ps}^{-1}\ ,$$

in good agreement with the input value.

Figure 9 gives the ratio:

$$\rho = \frac{N_{unlike\ sign} - N_{like\ sign}}{N_{unlike\ sign} + N_{like\ sign}}$$

for the data as a function of λ (summing the results from all sign indicators) together with the curve corresponding to the fitted value of Δm_d (a), the same without smearing the distribution of λ (see sect. 4) (b), the curve obtained with a time-independent mixing with a probability $\chi_d = 0.17$ (c) and the curve expected if no mixing occurs (d). At small values of λ the effect of the smearing (difference between (a) and (b)) is comparable to the difference induced by the oscillation itself, so that the fit could be dominated by systematic errors. However this effect is small in the range used in the fit ($\lambda > 2$ mm) where the data disagree with the no-mixing and time-independent-mixing hypotheses by 12 and 6 standard deviations respectively.

The likelihood fit was redone separately for each of the six combinations of tagging methods. The results are summarized in Figure 10 (after correction for a systematic effect due to the charged kaon multiplicities in B decays, as described below). The results are all compatible with the final combination, particularly if the systematic errors which are specific to kaons or leptons are taken into account. As an example, these contributions are completely uncorrelated in the ($l+j$ versus l) and (K+j versus K) subsamples: they are quadratically added to the statistical errors to give the dashed lines in Figure 10.

5.4.1 Sources of systematic uncertainty

The relative ratio of like and unlike sign correlations is expected to be a combination of (see Figure 11):

- almost equal numbers of like and unlike signs from $u\overline{u}$ and $d\overline{d}$ background.
- an $s\overline{s}$ contribution slightly favoring unlike signs (because of leading kaons having the sign of the initial quark).
- a more complex $c\overline{c}$ contribution where leptons and kaons from a c have opposite signs, resulting in opposite and same sign correlations when considering the sign indicators on both sides; the simulation indicates that they almost cancel each other.

- a non-oscillating b component, giving a large constant ratio favoring unlike sign pairs
- the oscillating component.

The probabilities of the light quark components decrease rapidly with λ whereas the $c\overline{c}$ probability varies less rapidly, but the non-b component is small after the cut on λ at 2 mm (see Figure 11, lower plot).

As the oscillation is seen over less than one period, the fitted value of Δm_d is mainly sensitive to the average of the ratio ρ from λ_{min} to ∞, weighted by the corresponding event rates. Hence it depends on the fraction of background and of the non-oscillating component (the shape of the oscillation is not constraining enough to allow a fit with freely varying fractions and lifetimes).

Parameter	Value	Variation	Effect on Δm_d (ps^{-1})
B_d^0 fraction	0.392	± 0.022	∓ 0.005
B_s^0 fraction	0.100	± 0.022	∓ 0.015
global B lifetime	1.567 ps	± 0.020 ps	$+0.002 \mp 0.001$
B_d^0 lifetime	1.57 ps	± 0.05 ps	$+0.004 \mp 0.006$
b fragmentation : $< p_B/p_{beam} >$	0.70	± 0.02	± 0.003
BR($b \to l$)	11.0%	$\pm 10\%$	± 0.010
BR($b \to c \to l$)	8.1%	$\pm 10\%$	∓ 0.013
K^+/K^- multiplicity in B decays	see text		-0.043 ± 0.042
Q_{jet}	see text		± 0.040
electron effic. and contamination	see text		± 0.008
muon effic. and contamination	see text		± 0.008
kaon effic. and contamination	see text		± 0.032
cut on ($\lvert\cos\theta_{thrust}\rvert$)	0.7	$0.7 \to 0.5$	< 0.020
parametrization	see text		± 0.011
fit procedure	see text		± 0.020
total			± 0.078

Table 9: *Systematic errors on* Δm_d.

The following effects have been taken into account to evaluate the systematic uncertainty on Δm_d.

- Fractions: the fractions of the different quark flavors produced from Z^0 decays are known with enough precision to give a negligible contribution. Larger effects can be expected from the uncertainties on the production rates of the various B hadrons. The B_d^0 and B_s^0 production rates were varied as detailed in section 4.3.
- Lifetimes: the simulation was done with the same lifetime for all B-hadrons. A common variation of all B lifetimes (± 0.02 ps) gives, as expected with a low $udsc$ background, only a small variation on Δm_d (± 0.001 ps^{-1}); on the contrary, a difference between $\tau_{B_d^0}$ and the other lifetimes makes the fraction of B_d^0 depend on λ, and then the ratio (like sign)/(unlike sign) is distorted. If only the simulated B_d^0 lifetime varies by ± 0.05 ps, the variation of Δm_d is ∓ 0.006 ps^{-1}. The difference between the values of the current B lifetimes and those used in the simulation (see Table 1) gives a correction of $+0.006$ ps^{-1} on Δm_d.

- Fragmentation: the B momentum spectrum was varied in such a way that the mean fraction of the beam momentum carried by each of the B hadrons, $< p_B/p_{beam} >$, was 0.70 ± 0.02. This gave a contribution of ± 0.003 ps^{-1}.
- Semileptonic branching ratios: the values of the semileptonic branching ratios used in the simulation were: $\mathrm{Br}(b \to l) = 11.0\%$, $\mathrm{Br}(b \to c \to l) = 8.10\%$. A relative variation of $\mathrm{Br}(b \to l)$ of $\pm 10\%$ gives ± 0.010 ps^{-1} on Δm_d , and $\pm 10\%$ on $\mathrm{Br}(b \to c \to l)$ gives ∓ 0.013 ps^{-1} on Δm_d.
- $\mathrm{K}^+/\mathrm{K}^-$ multiplicities in B decays: the values in the simulation used in this study differ slightly from the values measured in [17], so that the fitted value of Δm_d may be biased; to determine the correction and its uncertainty, weights were applied to the simulated events in order to reproduce each of the fractions $\mathrm{B}^+ \to \mathrm{K}^+ X$, $\mathrm{B}^+ \to \mathrm{K}^- X$, $\mathrm{B}^0_d \to \mathrm{K}^+ X$, $\mathrm{B}^0_d \to \mathrm{K}^- X$, measured in [17], and their uncertainties. As the effect of $\mathrm{B}^\pm$ was found to be predominant, it was not possible to take advantage of the fact that the fractions averaged over $\mathrm{B}^\pm$ and B^0_d have been measured with a better precision. Finally the correction on Δm_d was evaluated to be -0.043 ± 0.042 ps^{-1} (with a quadratic addition of the uncertainties from the four B$\to$ K fractions).
- Jet charge (including detector effects): the probability p of finding the right "production" sign from Q_{jet} was cross checked on data by comparing the charges measured in opposite hemispheres. The fraction of events with unlike signs, expected to be $p^2+(1-p)^2$ if p is the same for all flavors, was evaluated both for the data and for the simulated hadronic events. This was done using different non-overlapping ranges of the b-tagging variable C_b described in section 5.1. The p values for the real data and for the simulated event samples were compared in each case (see Figure 12). They were typically found to be compatible within ± 0.005. However the extrapolation to pure $b\overline{b}$ samples both increases the statistical uncertainty of the comparison and also depends on the assumed fractions of B^0_s and b-baryons. This increased the uncertainty on the p values used in the fit to ± 0.010, giving a variation of ± 0.040 ps^{-1} on Δm_d.
- Lepton identification: changing the electron identification efficiency by $\pm 5\%$ changes the fitted value of Δm_d by ± 0.008 ps^{-1}; changing by $\pm 10\%$ the hadron misidentification probability gives ± 0.002 ps^{-1} for Δm_d. For muons, the corresponding uncertainties induced on Δm_d are ± 0.007 and $\pm\, 0.005$ ps^{-1}.
- Kaon identification: the uncertainty in the kaon identification efficiency of the RICH was estimated to be $\pm 10\%$; the effect on Δm_d is ∓ 0.016 . A margin of $\pm 30\%$ on the contamination by pions gives ± 0.028 ps^{-1}on Δm_d.
- Geometrical acceptance: to check possible edge effects in the acceptance of the RICH detector, the range on $|\cos(\theta_{thrust})|$ was reduced in steps from 0.7 down to 0.5; the corresponding uncertainty on Δm_d is estimated to be less than 0.020 ps^{-1}.
- Parametrization: there are statistical uncertainties on $\mathcal{P}_{tag}^{right/wrong}$ and $\mathcal{P}_{dec}^{right/wrong}$, and on the parametrizations of $\mathcal{P}_{cat}(\lambda)$ and $\mathcal{P}_{osc}(\lambda)$. By splitting the simulated events sample into ten subsamples and computing with each of them an independent set of coefficients, the observed dispersion of the fitted Δm_d values was 0.024 ps^{-1}. The uncertainty for the total sample is then estimated to be 0.008 ps^{-1}. The smearing introduced in the resolution function of the distance estimator (see sect. 5.2) modifies the parametrization of the functions $\mathcal{P}_{cat}(\lambda)$. The fitted value of Δm_d is then moved by 0.007 ps^{-1}. These two effects contribute ± 0.011 to the systematic error.
- Fit procedure: In some events, the decay distance was measured in both hemispheres. In consequence, 11% of the events occur twice in the fitting sample. As the two entries correspond to independent values of λ, the information is not completely

redundant. In order to estimate the effect of this partial double counting on the statistical error, several hundred samples were generated with a simplified simulation reproducing the fractions, tagging probabilities and time dependences used in the fit, independently in each hemisphere, and each such sample was fitted separately; the dispersion of the fitted values showed that the true statistical error was $5\pm3\%$ higher than the error given by MINUIT when including the double entries. In addition, some 1.5% of b hemispheres had both a kaon and a lepton in the same hemisphere and in agreement with Q_{jet}. These were also counted twice. It was found that the alternative procedure of removing hemispheres with both a kaon and a lepton if the signs were opposite, or defining a separate indicator if they were the same, gave a 5% smaller statistical error and a shift of 0.020 ps. Both of these effects were therefore accounted for by a further systematic error of ±0.020 ps.

- Choice of λ_{min}: the fit was redone with different values of λ_{min} between 1 and 4 mm. The result was stable (see Figure 13). The dispersion of the results is compatible with the statistical fluctuations, and the systematic error is estimated to be less than 0.020 ps^{-1}.

Table 9 summarizes the contributions to the total systematic uncertainty on Δm_d. Taking into account the corrections due to differences in lifetime values and in the charged K rates in B meson decays between data [17] and the simulation, the measured value of Δm_d is then:

$$\Delta m_d = 0.531^{+0.050}_{-0.046}\ (stat.) \pm 0.078\ (syst.)\ \text{ps}^{-1}\ .$$

6 Conclusions

The time-dependent $\mathrm{B}^0_d - \overline{\mathrm{B}^0_d}$ oscillations have been measured from the distributions of high p_t lepton impact parameter obtained separately for same sign and opposite sign dilepton events:

$$\Delta m_d = 0.47 \pm 0.08\ (stat.)^{+0.09}_{-0.08}\ (syst.)\ \text{ps}^{-1}\,.$$

The analysis has been extended to include charged kaons from secondary vertices and the mean jet charge to tag the produced and decaying B mesons giving:

$$\Delta m_d = 0.531^{+0.050}_{-0.046}\ (stat.) \pm 0.078\ (syst.)\ \text{ps}^{-1}$$

or equivalently:

$$\Delta m_d = (3.49^{+0.33}_{-0.30} \pm 0.52)10^{-4}\ \text{eV}/c^2\,.$$

Using the averaged value of $\tau_{B^0_d} = 1.57 \pm 0.05$ ps [11] this gives:

$$x_d = \Delta m_d/\Gamma = 0.83^{+0.08}_{-0.07} \pm 0.13\,.$$

The data deviate from the hypothesis of a time-independent mixing (with a probability $\chi_d = 0.17$) by 6 standard deviations.

Acknowledgements

We are greatly indebted to our technical collaborators and to the funding agencies for their support in building and operating the DELPHI detector, and to the members of the CERN-SL Division for the excellent performance of the LEP collider.

References

[1] A.J. Buras, W. Slominski and H. Steger, Nucl. Phys. **B245** (1984) 369.

[2] ARGUS Coll., H. Albrecht et al., Phys. Lett. **B324** (1994) 249;
CLEO Coll., J. Bartelt et al., Phys. Rev. **D50** (1994) 43;
ALEPH Coll., D. Decamp et al., Phys. Lett. **B284** (1992) 177;
DELPHI Coll., P. Abreu et al., Phys. Lett. **B332** (1994) 488;
L3 Coll., M. Acciarri et al., Phys. Lett. **B335** (1994) 542;
OPAL Coll., R. Akers et al., Zeit. Phys. **C60** (1993) 199;
R. Aleksan, plenary review talk at the ICHEP95 Conference, Brussels, July 1995;
S-L. Wu, plenary review talk at the XVII Int. Lepton-Photon Symposium, Beijing, August 1995.

[3] ALEPH Coll., D. Buskulic et al., Phys.Lett. **B313** (1993) 498;
ALEPH Coll., D. Buskulic et al., Phys.Lett. **B322** (1994) 441;
DELPHI Coll., P. Abreu et al., Phys. Lett **B338** (1994) 409;
OPAL Coll., R. Akers et al., Phys. Lett. **B327** (1994) 411;
OPAL Coll., R. Akers et al., Phys. Lett. **B336** (1994) 585.

[4] DELPHI Coll., P. Aarnio et al., Nucl. Instr. and Methods **A303** (1991) 233.

[5] DELPHI Coll., P. Abreu et al., *Performance of the DELPHI Detector*, CERN-PPE/95-194, to be published in Nucl. Instr. and Meth. A.

[6] N. Bingefors et al., Nucl. Instr. and Methods **A328** (1993) 447.

[7] E.G. Anassontzis et al., Nucl. Instr. and Methods **A323** (1992) 351.

[8] T. Sjöstrand, Comp. Phys. Comm. **27** (1982) 243; ibid. **28** (1983) 229;
T. Sjöstrand, M. Bengtsson, Comp. Phys. Comm. **43** (1987) 367.

[9] DELSIM Reference Manual, DELPHI internal note, DELPHI 87-97 PROG-100.

[10] DELPHI Coll., *Tuning and Test of Fragmentation Models Based on Identified Particles and Event Shape Data*, Contributed paper eps0548 to the ICHEP95 Conference, Brussels, July 1995, and paper to be submitted to Z. Phys. **C**.

[11] S. Komamiya, plenary review talk at the ICHEP95 Conference, Brussels, July 1995.

[12] N. Isgur, D. Scora, B. Grinstein and M. Wise, Phys. Rev. **D39** (1989) 799.

[13] DELPHI Coll., P. Abreu et al., Zeit. Phys. **C65** (1995) 569.

[14] P. Billoir and S. Qian, Nucl. Instr. and Methods **A311** (1992) 139.

[15] ALEPH Coll., Contribution to ICHEP94 Conference (Glasgow, July 1994);
ALEPH Coll., Contribution to the ICHEP95 Conference, Brussels, July 1995;
DELPHI Coll., P. Abreu et al., Phys. Lett. **B332** (1994) 488;
DELPHI Coll., Contribution to ICHEP95 Conference, Brussels, July 1995;
L3 Coll., M. Acciarri et al., Phys. Lett. **B335** (1994) 542;
OPAL Coll., R. Akers et al., Zeit. Phys. **C60** (1993) 199;
OPAL Coll., R. Akers et al., Zeit. Phys. **C66** (1995) 555;
OPAL Coll., R. Akers et al., Phys. Lett. **B336** (1994) 585;
OPAL Coll., Contribution to the Moriond 1995 Conference.

[16] ARGUS Coll., H. Albrecht et al., Phys. Lett. **B207** (1988) 109; Phys. Lett. **B269** (1991) 243; Phys. Lett. **B274** (1992) 239; Zeit. Phys **C56** (1992) 1;
CLEO Coll., P. Avery et al., Phys. Rev. **D43** (1991) 3599; Phys. Rev. Lett. **65** (1990) 2842.

[17] ARGUS Coll., H. Albrecht et al., Zeit. Phys. **C62** (1994) 371.

[18] DELPHI Coll., P. Abreu et al., Phys. Lett. **B322** (1994) 459.

[19] F. James, MINUIT, Function Minimization and Error Analysis, Reference Manual, version 94.1, CERN Program Library Long Writeup D506.

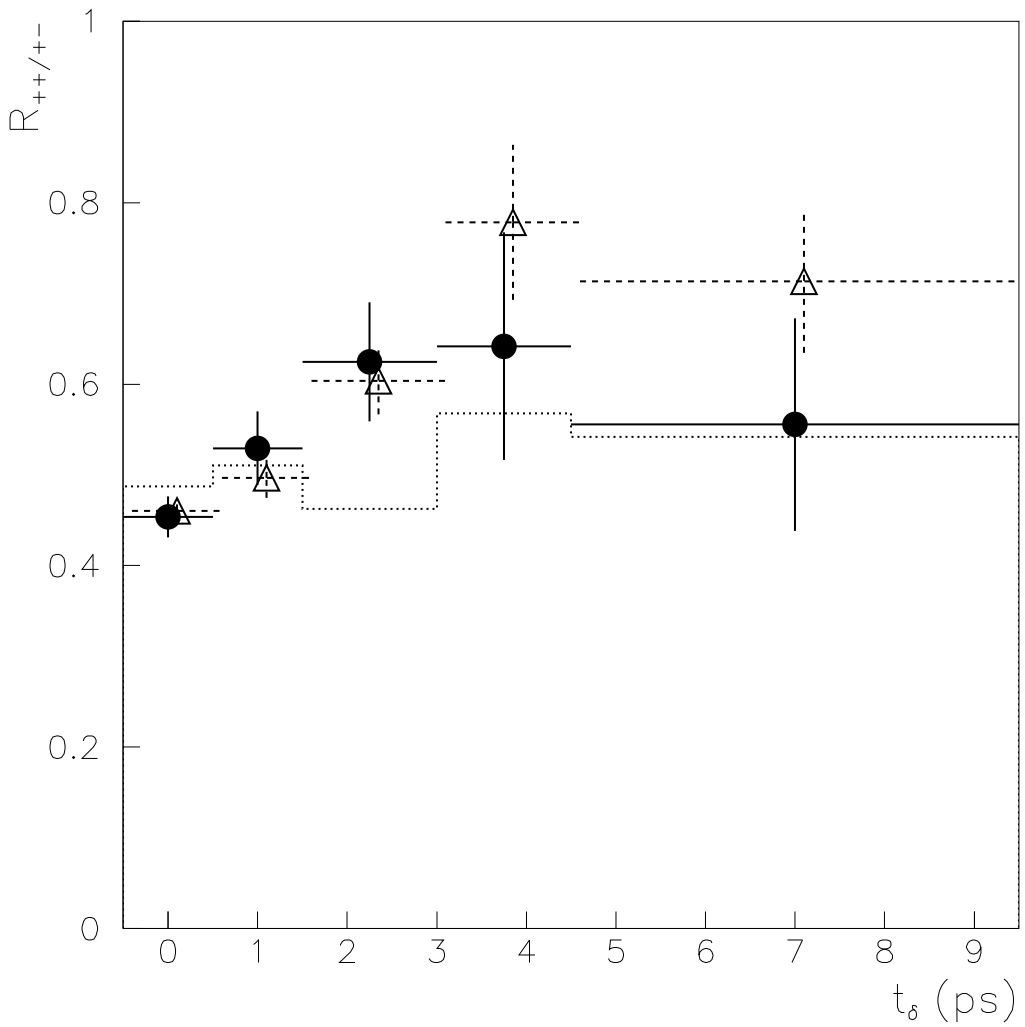

Figure 1: Ratio $R_{++/+-}$ of the t_δ distributions obtained from same sign and opposite sign dilepton events when both leptons have a p_t greater than 1 GeV/c. Black circles correspond to real data events, triangles to simulated events with $\Delta m = 0.47$ ps^{-1}. The dotted histogram corresponds to the hypothesis of time independent mixing.

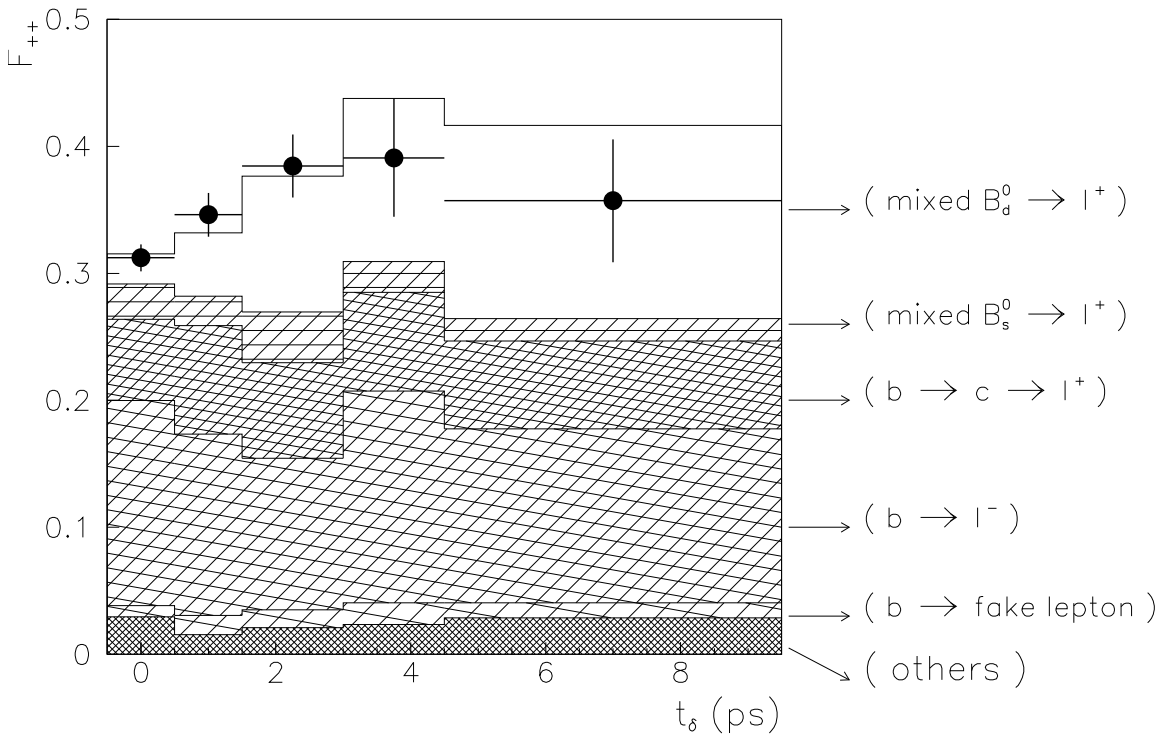

Figure 2: Fraction F_{++} of same sign correlations obtained when both leptons have a p_t greater than 1 GeV/c, with the contribution from the various sources according to the simulation.

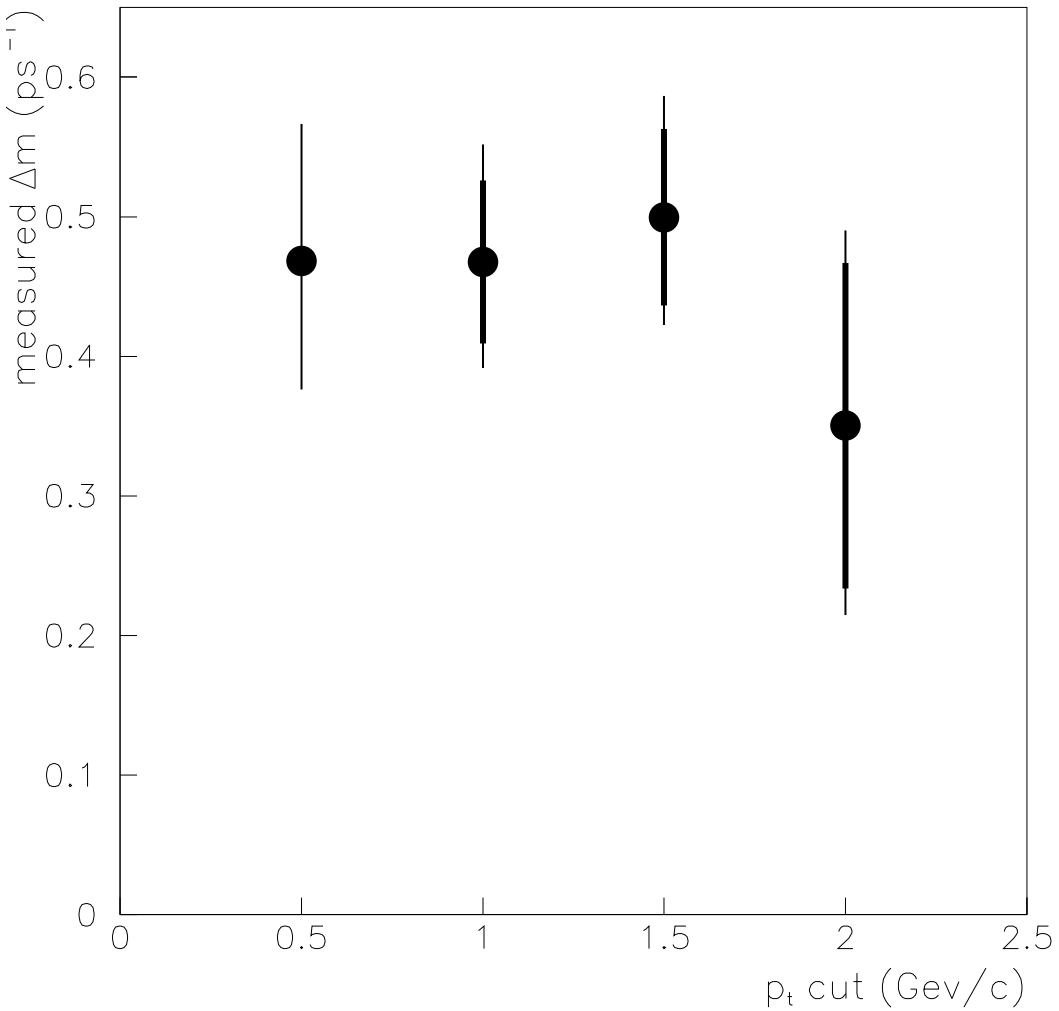

Figure 3: Δm_d values measured for different p_t cuts. The thin error bars show the total statistical errors. The thick error bars show the error on the difference between the given point and the adjacent one for a smaller p_t cut.

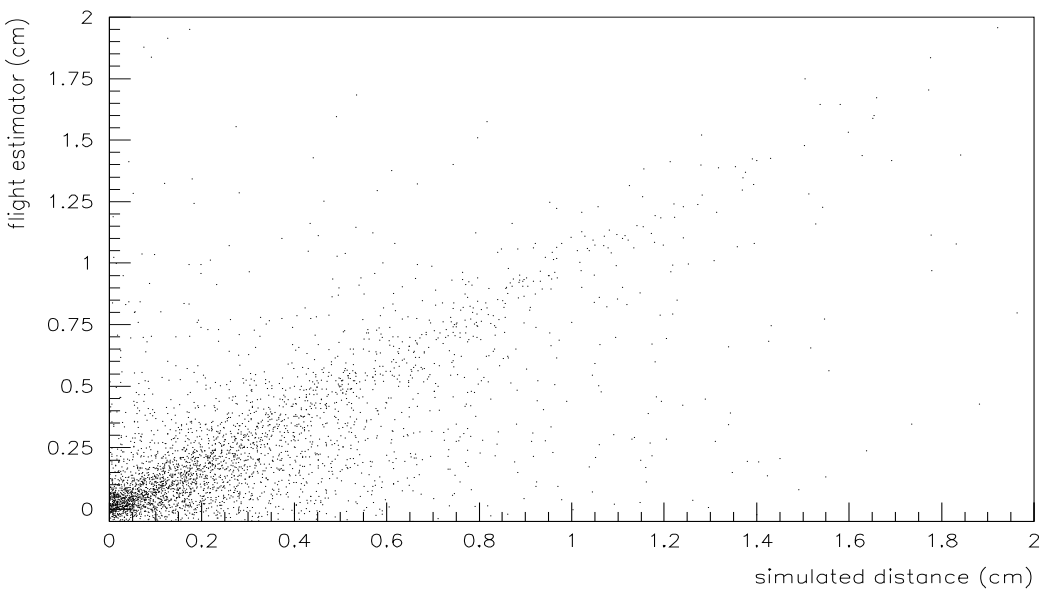

Figure 4: Comparison of the flight distance estimator λ with the true flight distance of the B hadron in simulated b hemispheres.

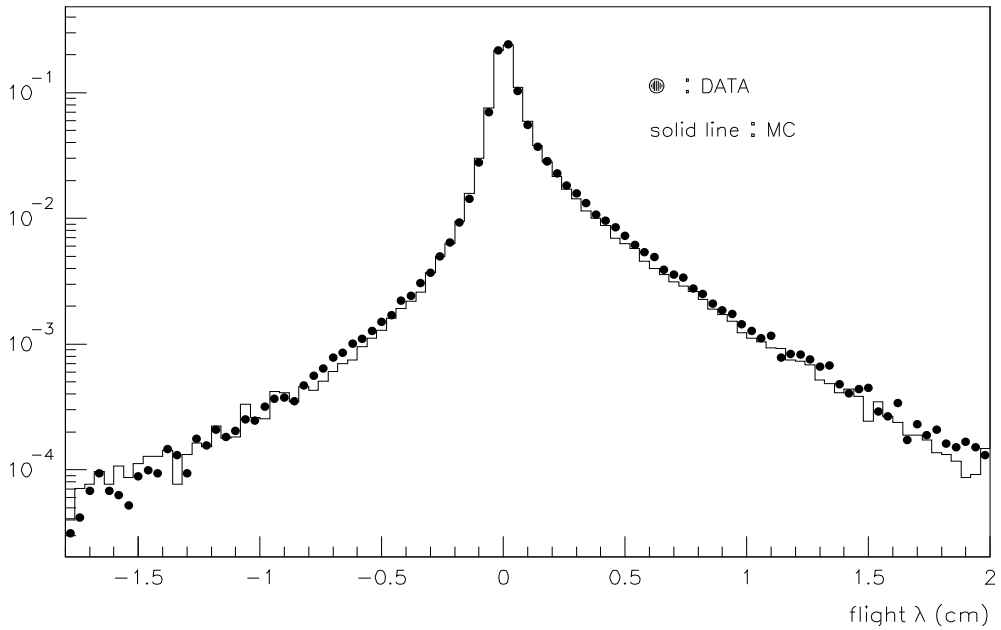

Figure 5: Comparison of the distribution of the decay distance λ in real and simulated data after applying the additional smearing as explained in section 5.2.

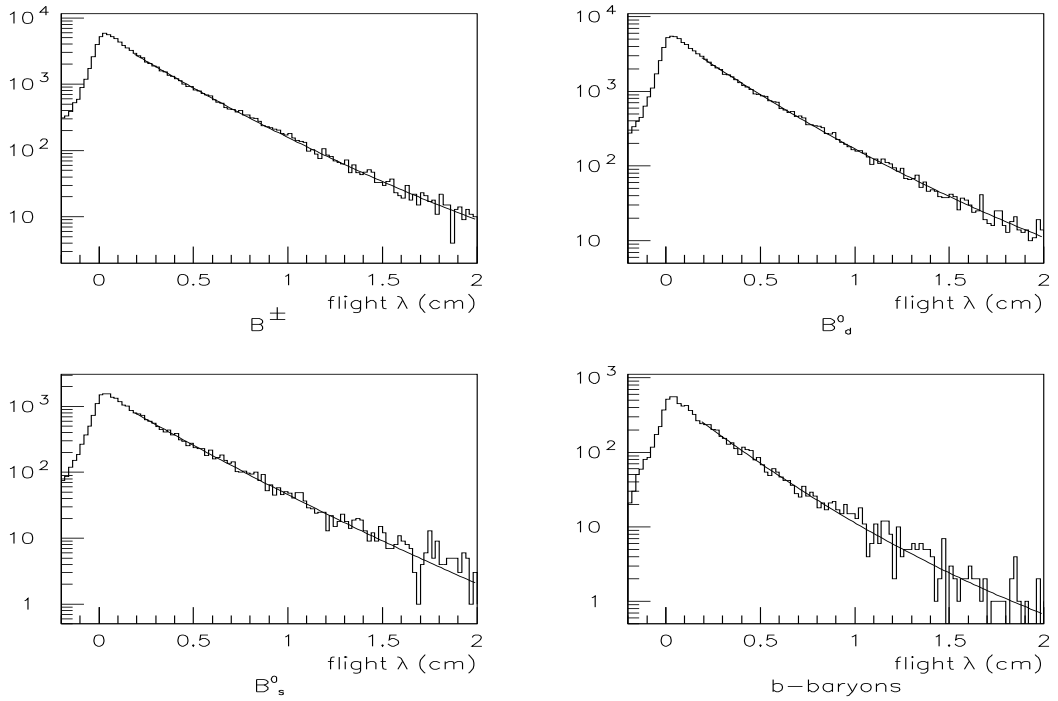

Figure 6: Distribution of the flight distance estimator λ for different b categories; the curves show the parametrization for $\lambda > 2$ mm.

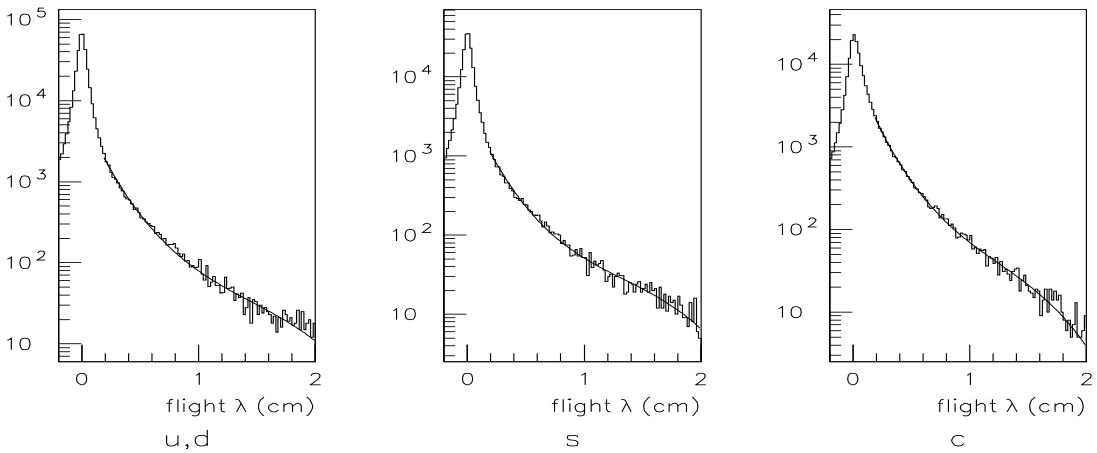

Figure 7: Distribution of the flight distance estimator λ for u/d, s and c categories; the curves show the parametrization for $\lambda > 2$mm.

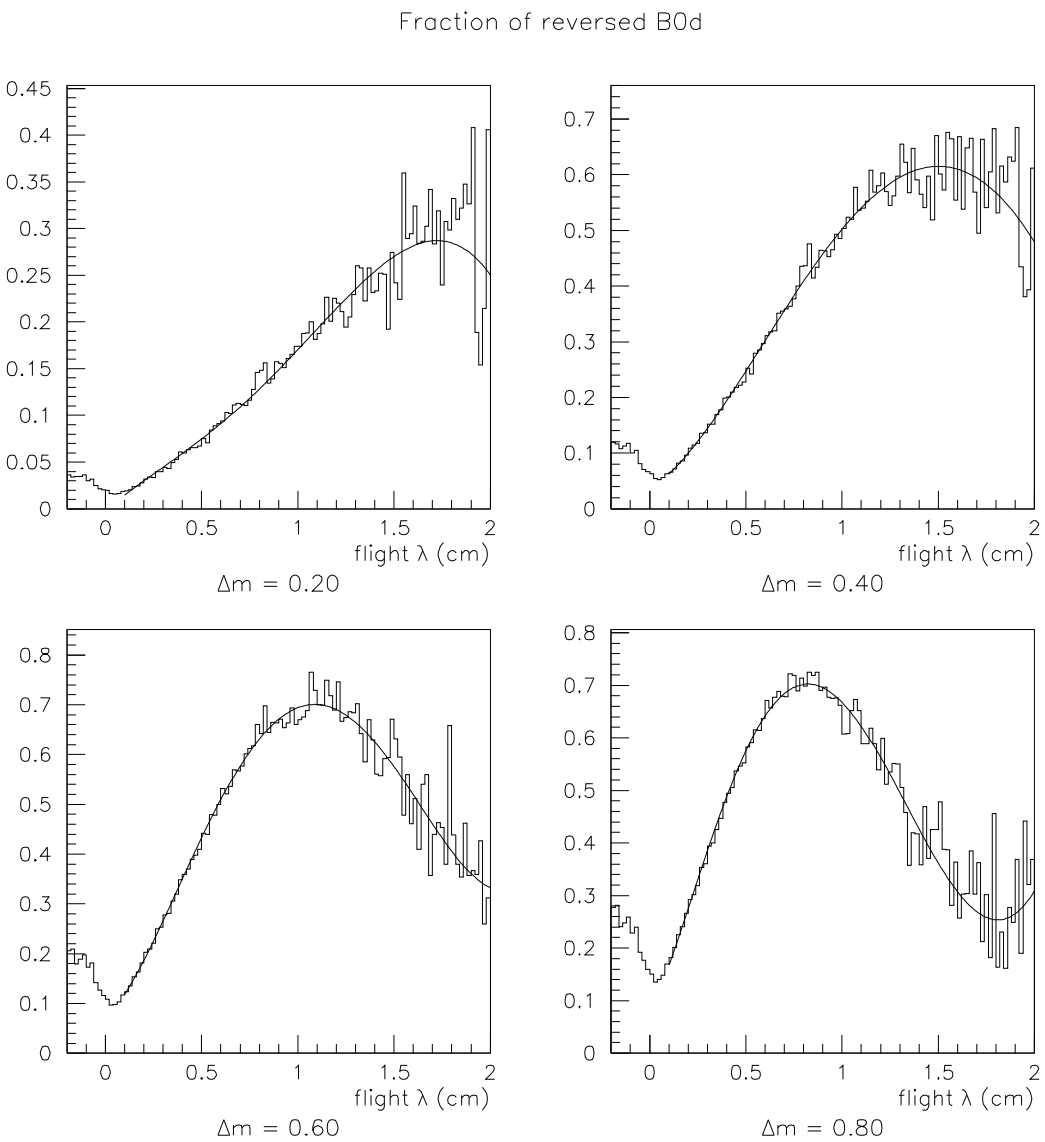

Figure 8: Probability of B^0_d oscillation as a function of the flight distance estimator λ. The curves show the parametrization described in the text for different values of Δm_d.

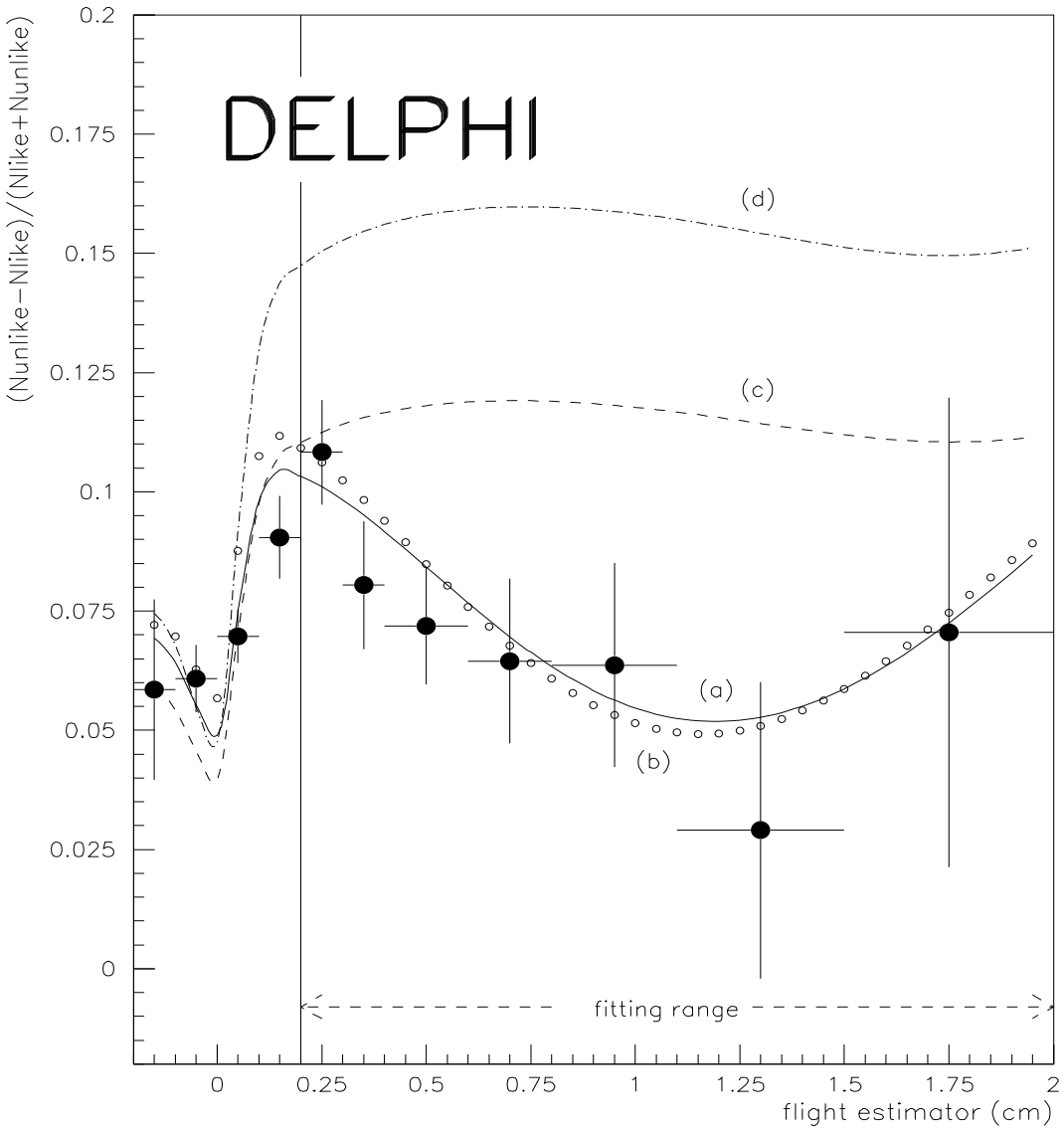

Figure 9: Ratio $(N_{unlike\ sign} - N_{like\ sign})/(N_{unlike\ sign} + N_{like\ sign})$ as a function of λ. The curves are the expected shapes for (a) the fitted time-dependent oscillation (full curve), (b) the same without smearing the values of λ (open circles), (c) a time-independent mixing with $\chi_d = 0.17$ (dashed curve), and (d) no mixing (dot-dashed curve).

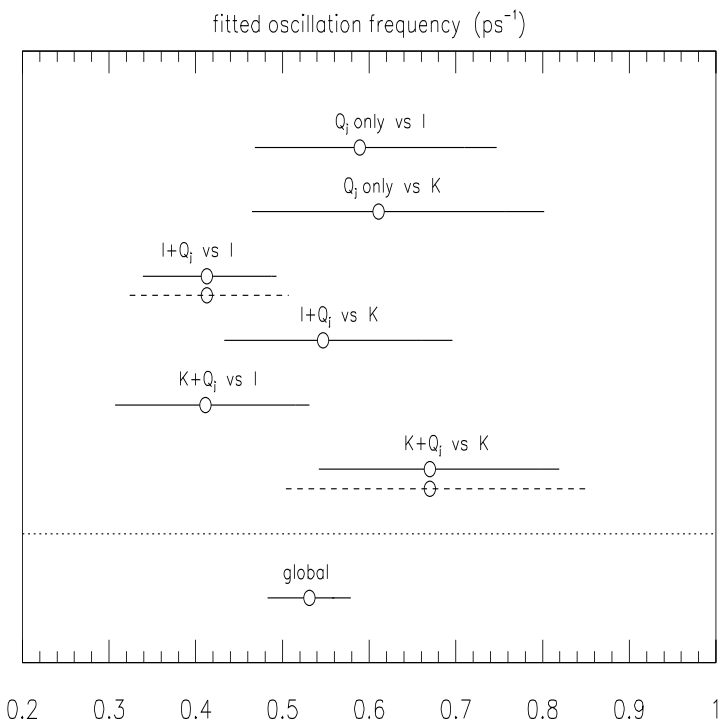

Figure 10: Values of Δm_d obtained for different combinations of the sign indicators. The dashed error bars show, for the two results whose systematic errors are least correlated, the effect of adding the uncorrelated systematic errors in quadrature.

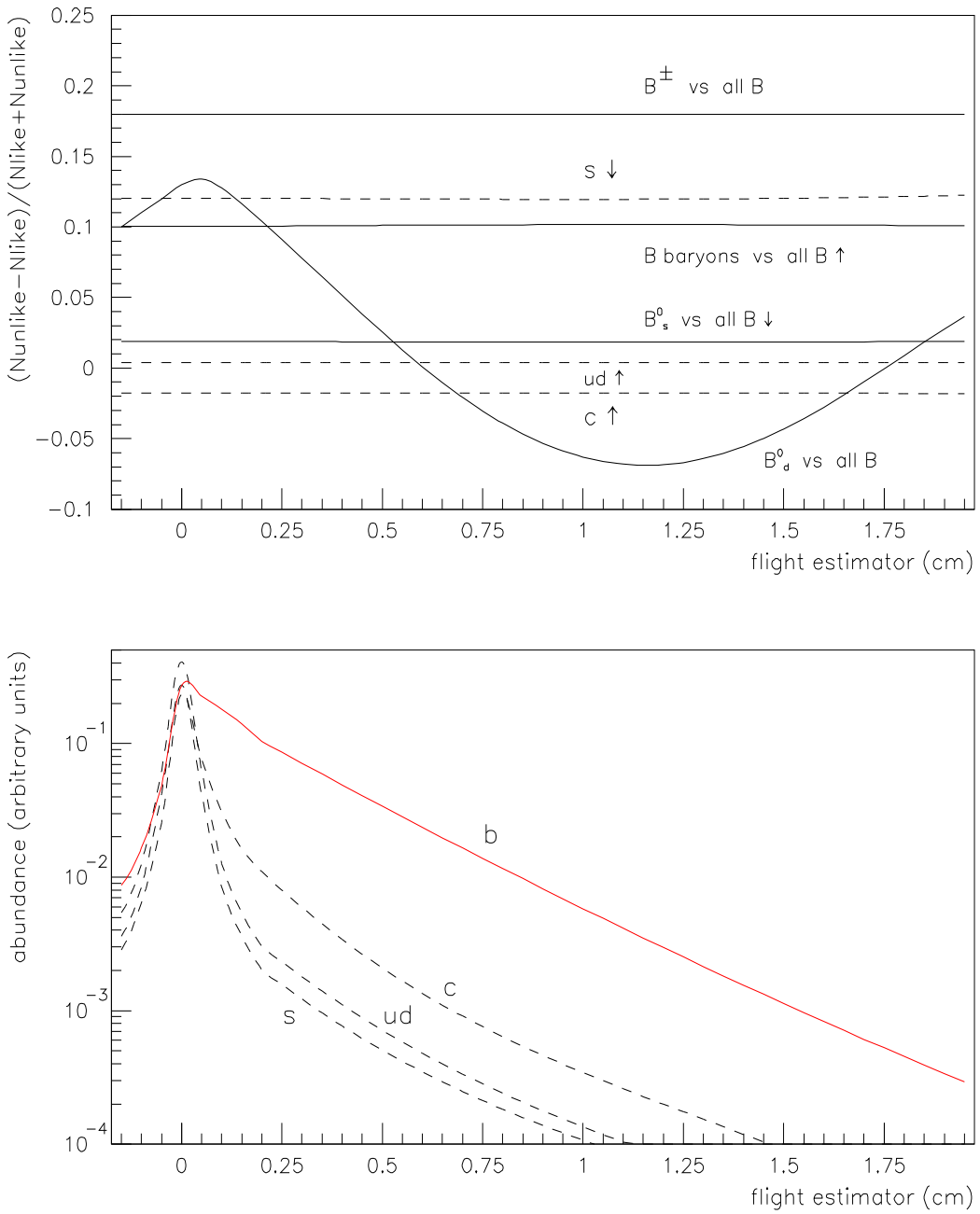

Figure 11: Upper plot: the value of ρ (see section 5.5) predicted by the simulation as a function of the flight distance estimator λ for different B hadrons in the decay hemisphere averaging over all types of B hadrons in the tagging hemisphere (full lines and curve), and for light quark pairs (dashed lines). Lower plot: the abundances of the different flavours in the fitted sample as functions of λ. The full curve in Fig. 9 is the sum of the predicted values of ρ in the upper plot weighted according to the predicted quark abundances shown in the lower one and the assumed B hadron fractions in b quark jets.

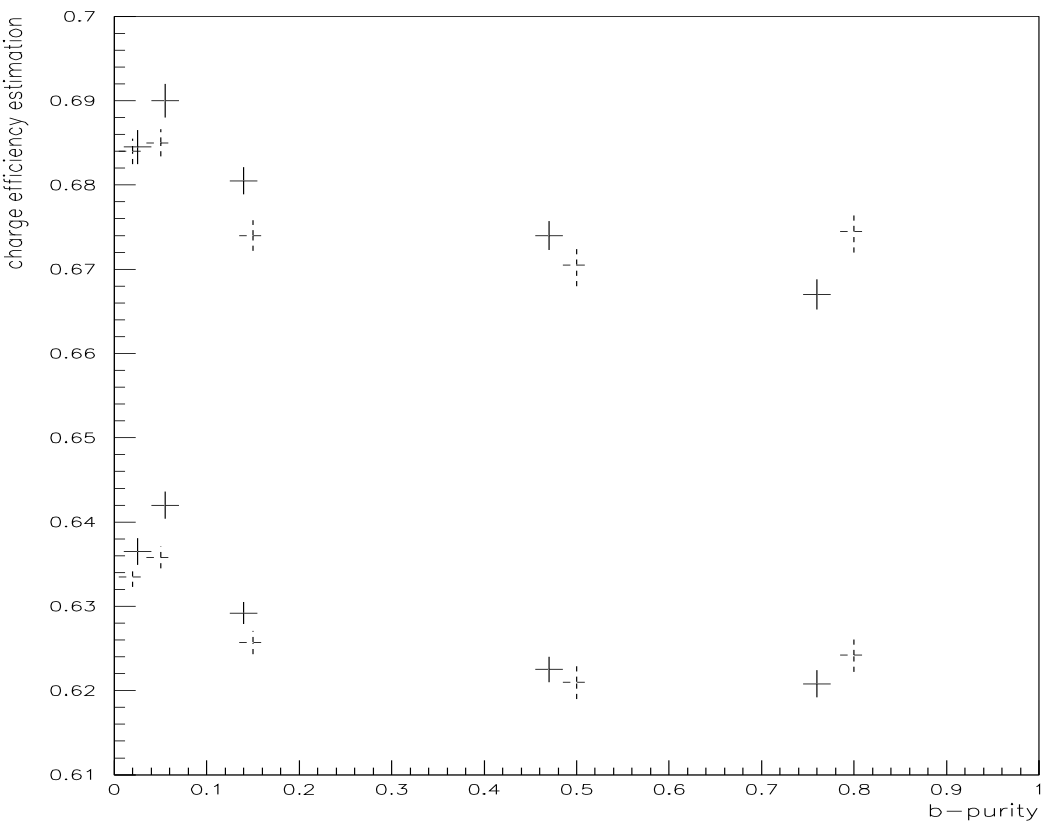

Figure 12: Comparison of jet charge sign efficiency between simulated and real data as a function of the b-purity of the sample. The samples are defined by cuts on the b-tag variable C_b defined in section 5.1, and do not overlap. The jet charge efficiency p for each sample is computed by assuming the fraction of unlike-sign hemispheres to be $p^2+(1-p)^2$. The solid lines correspond to real data, the dashed ones to simulation. The lower set of values is obtained keeping all values of Q_{jet}, as for the *(j+l)* and *(j+K)* indicators, and the upper set requiring $|Q_{jet}| > 0.1$ as for the *(j+btag)* indicator.

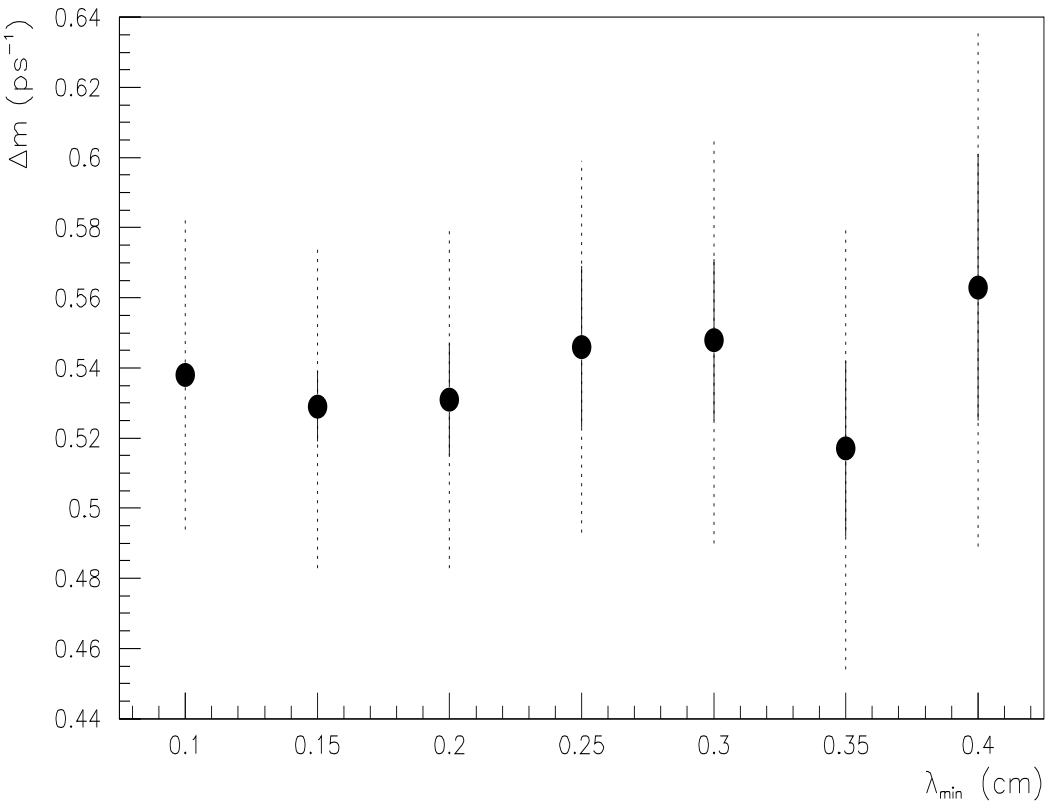

Figure 13: Fitted value of Δm_d for different values of λ_{min}. The dotted error bars show the total statistical errors. The full error bars show the error on the difference between the given point and the adjacent one at smaller λ_{min}.